Chapter 8

Forward Straw Detector

8.1 Introduction

This Chapter describes the Straw Detector which together with the Forward Silicon Tracker forms the the forward charged particle tracking system. The major functions of the forward tracking system are to provide high precision momentum measurements for tracks found in the pixel system, to reconstruct and measure all parameters for tracks which do not pass through the vertex detector (such as K_s and Λ^0 daughter tracks), and to project tracks into the RICH counters, EM calorimeters, and Muon detectors.

8.2 Requirements

The requirements of the Straw Detector are:

- Provide tracking coverage in each arm of the BTeV detector from the outer edge of the Forward Silicon Tracker out to 300 mrad.
- Provide robust pattern recognition for charged particles in conjunction with the pixel detector.
- Achieve a momentum resolution of $\sim 1\%$ for 100 GeV tracks. This can be achieved with a position resolution of 150μm.
- Material budget as low as possible ($\sim 1\%$ X_0/station) to minimize multiple scattering, energy loss, secondary interactions, and photon conversions.
- Drift time less than 132 nsec. Although the Tevatron will probably operate with a time of 396 nsec between bunch crossings we allow for the possibility of running with 132 nsec between bunch crossings.
- Be able to operate at a luminosity of 2×10^{32} cm^{-2} s^{-1} for 10 years.
- Be mechanically robust and modular so it can be installed around the beam pipe.

8.3 Baseline Design

The baseline forward tracking system consists of 7 stations, placed transversely to the beam at various distances from the interaction point. Three stations are placed in the dipole magnet, three stations in the field-free region just upstream of the RICH, and one station just downstream of the RICH. The entire system extends over a distance of $\sim$ 7 m and provides θ-angle coverage from $\sim \pm 10$ mrad up to ± 300 mrad.

The design of the forward tracking system has been driven by the high density of tracks produced in the forward direction, especially with multiple interactions per crossing. Most of the solid angle is instrumented using straw tube drift chambers. Straws have been chosen because they can be used to make large chambers with small cell size, and because they can be built to surround the beam pipe without requiring a heavy frame near the beam. The track density very close to the beam requires detectors with even higher granularity; we have chosen to instrument the central section of each station with silicon microstrip detectors.

The forward straw tube tracker consists of stations that provide 3 coordinate measurements, X, U and V, where the two stereo views, U and V, are at $\pm$ 11.3^o around the Y bend coordinate. With three layers per view, this configuration provides excellent resolution in the bend plane while maintaining a robust ability to reject ghost combinations of hits. It has sufficient redundancy to achieve a high detection efficiency and to resolve the left/right ambiguity a very large fraction of the time.

The unit of construction is the 'module' consisting of forty-eight straws of 4 mm diameter, arranged in three rows of 16. (We are considering the use of 8 mm straws in the low occupancy regions.) The modules are then assembled in a frame to form a 'half-view'(Fig. 8.1). Three sides of the frame are made of aluminum extrusions. On the fourth side, which is in the active area of the detector, the tension is supported by a low mass carbon fiber strut. In the region around the beam-pipe, straws are terminated at a carbon fiber gas manifold. In order to keep the straws at a constant humidity we plan to flow dry nitrogen in a volume surrounding the straws.

All the sense wires for the straws that do not terminate at the central gas manifold are divided electrically using a small glass capillary bead following the technique used for the ATLAS TRT [1]. This cuts the occupancy rates in half. In addition, within a 26 cm square region around the beam-pipe, all sense wires will use 2 capillary beads to deaden the central section of the wire. This region is covered by the Silicon Strip Tracker.

Table 8.1 lists all the geometric parameters and the main characteristics of the Straw Detector.

8.4 Detector Components

8.4.1 Module Description

Straws are assembled in groups called modules. A module contains either 48 straws of 4 mm diameter or 16 straws of 8 mm diameter. A module consists of a group of straws containing

Figure 8.1: Straw Detector Half-View

Table 8.1: Properties of the baseline forward Straw Detector

Property	Value
Straw size	4 mm diameter
Central hole	26 cm × 26 cm
Total Stations	7
Z positions (cm)	96, 138, 196, 288, 332, 382, 725
Active Half size (cm)	28.0, 42.0, 63.0, 91.0, 105.0, 119.0, 189.0
Views per station	3 (X,U,V)
Layers per view	3
Total number of straws	26208
Total station thickness	0.9% X_0
Total channels	52416
Readout	ASDQ + TDC (6 bits), sparsified

wire centering devices and mounted to two end plates. Straws and endplates are aligned to each other during module assembly. The end plates have alignment holes that allow modules to be aligned properly when mounted to the frame of the Half-view assembly. Fig 8.2 shows a module on the module assembly fixture.

The components of a module are the straws, twisters (wire centering device), end plugs and end plates. Straws are electrically and structurally connected to the end plates with electrically conductive epoxy and structural epoxy.

Straws are assembled into modules primarily for production benefits. However, the use of modules also provides an option for replacing damaged straws prior to the installation of the half-view frame. The primary production benefit of modules comes from the ability to make the structural, electrical and alignment connection to a significant number of straws with each bonding operation. Epoxy bonds can be made simultaneously without concern for excess epoxy affecting the close packing of adjacent straws. The use of modules also allows the operation of bonding to straws to be decoupled from the assembly and wiring of half-view frames.

The straws and end plates are aligned to each other with a module assembly fixture and that alignment is fixed by the electrically conductive epoxy that attaches the straws to the end plate. The end plugs aid the structural connection and gas seal of the straws to the end plates but they do not set the alignment.

The straw module closest to the beamline is physically two modules attached to a carbon fiber manifold which surrounds the beampipe (see section 8.4.4.5.

Figure 8.2: Straw Module

8.4.2 Module Components

8.4.2.1 Straws

The basic detecting element is the straw – a tube made by winding two strips of thin film ($\sim$ 1 cm wide) around a mandrel. The final choice of material will be made when we have finished testing both mechanical properties and radiation aging.

The original prototype straw tube was developed by the University of Indiana, based on the design of the Atlas straws. An aluminum conduction layer is placed between two

Kapton films, the inner one next to the gas volume being a carbon loaded, low resistivity film (Kapton XC) to form a protective barrier. We measured the surface resistivity of the aluminum coated, carbon loaded Kapton film of this prototype to be 0.5Ω/square.

The other options for straw material are copper coated kapton and copper coated mylar.

8.4.2.2 Signal Wire, Wire supports – twisters

The sense wire for the straw cells is 25 micron diameter gold plated tungsten held under 50 grams of tension. In addition, the sense wires will be divided electrically using a small glass capillary bead [1]. This cuts the occupancy rates in half.

The wire-centering device is called a twister (see Fig 8.3). Twisters were proposed for the SSC SDC Tracker detector and have been used in the construction of the ATLAS TRT detector. The twister is machined from Ultem®1000 plastic. The helix of the twister centers the wire in the straw but allows free flow of gas past the twister. The outside diameter of the twister is nominally 25 μm smaller than the inside diameter of the straw. The twister is held in place by a low melting point thermoplastic adhesive that has been applied to the outside of the twister prior to insertion in the straw. After the twister has been inserted and positioned, the adhesive is re-softened by blowing hot air over the outside of the straw.

Ultem (polyetherimide) was selected for the twister material based on testing and evaluations made for the ATLAS TRT detector. Ultem has almost the same radiation hardness as polyimide and PEEK materials but has better adhesion properties.

Twister dimensions will be inspected by sampling from batches and measuring the position of a wire strung through the twister. Figure 8.4 shows the fixture used for inspecting prototype twisters. It was learned during the prototype phase that small burrs on the ends of the twister could lead to wire alignment problems. Prototype twisters have been obtained from two vendors that meet specifications.

Twisters are located at the ends of the straws. They are also located at intermediate positions so that that any unsupported length of anode wire is no greater than 80 cm.

8.4.2.3 End Plugs

End plugs are fabricated from the same Ultem®1000 plastic as the twister. The end plug is stepped in diameter to allow for the close packed connection of the straws and module end plate (see Fig 8.5). The anode wire passes freely through the end plug with the alignment of the wire being controlled by the adjacent twister. The end plug serves the following functions. It provides the structural connection of the straws to the module end plate. It acts as an insulator between the anode wire and the grounded end plate. It presents a restriction in gas flow to provide for balanced flow among all straws in a module. The ends of the end plugs are tapered to assist passage of the anode wire and lead wire as it is blown through the straw during wire stringing.

The prototype end plugs have been machined. The lower tolerance of the end plug may permit the production parts to be fabricated by injection molding. Ultem is an injection

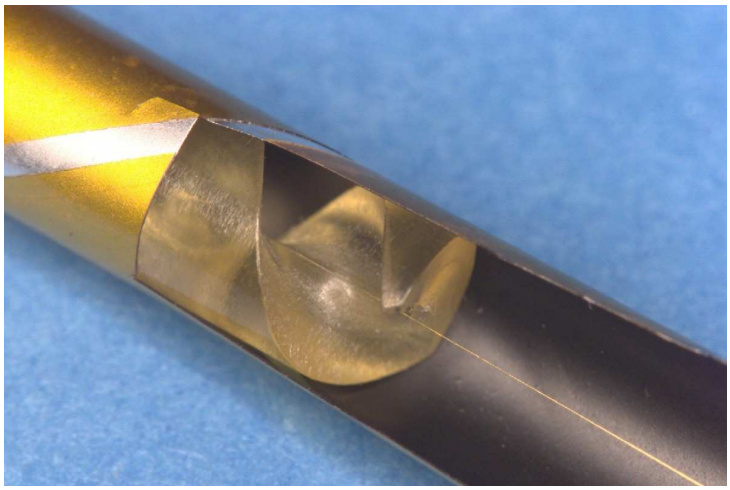

Figure 8.3: Straw cut away to show twister and anode wire

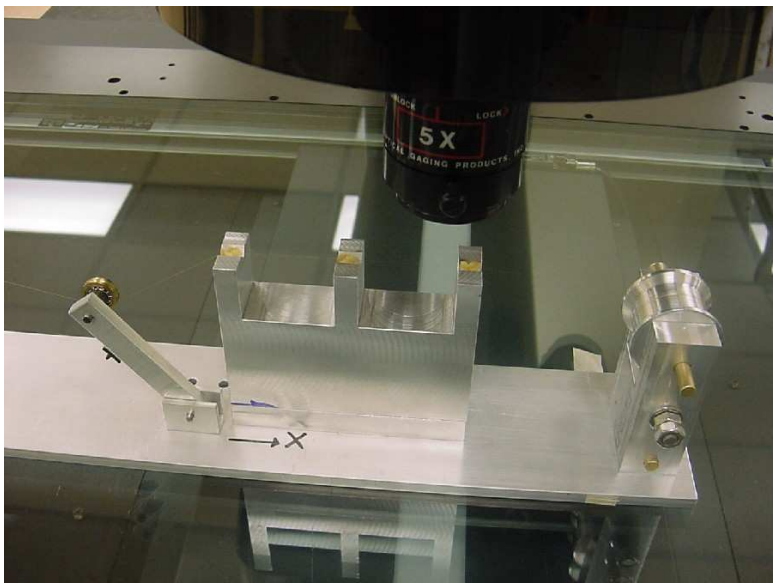

Figure 8.4: Twister Inspection fixture

moldable thermoplastic. Molding issues such as mold part lines and mold release agents will need to be investigated before a decision about molding of the end plugs can be made.

8.4.2.4 Module End Plate

The module end plates are made from aluminum alloy. The material was selected for machining properties and weight. In prototypes, no problems have been encountered in maintaining

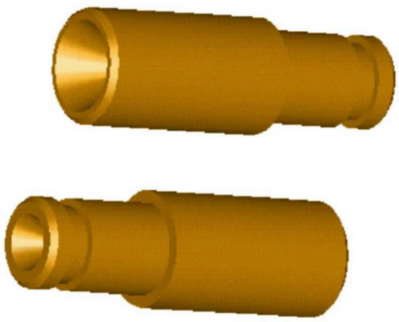

Figure 8.5: Endplugs

electrical contact with the aluminum end plate. The left and right end plates of a module are mirror images of one another. The end plate has four tapped holes and two precision holes that are used to mount and align the module to the half-view frame. The front face of the end plate has a recessed pocket where the tips of the end plugs extend.

The module end plates for stations 1 and 2 are different from all other end plates (see Fig 8.6). Because of space constraints within the vertex magnet, the ends of the half-view frames of the U and V views must be 11.3^o from perpendicular with the axis of the straws. To accommodate this angle, the module end plate design is modified. The holes for the end plugs are at an angle of 11.3^o from perpendicular and the back face of the end plate is shingled. The shingled face provides a surface that is perpendicular to the end of the straw and the shoulder of the end plug.

8.4.3 Half-view frame description

The half-view frame is the structure that holds and aligns the modules for one view of a station. The half-view frame designs for stations 3,4,5 and 6 are very similar and scale in height and width for the coverage of the station. The half-view frame designs for stations 1 and 2 are similar to 3-6 except that the long and short sides attach at 11.3^o from perpendicular. Station 7 has a different design based on super-modules (see section 8.4.6).

The straw modules are attached to the short sides of the half-view frame. The short sides are made from aluminum extrusions. They contain the front-end readout electronics. They also contain internal channels for cooling the electronics and maintaining the frame at a constant temperature to achieve the required dimensional stability. The chamber gas is distributed to the straw modules through passages in the frame. Fig. 8.7 shows a detail of the modules installed in a half-view frame.

The half-view frame holds the tension in the straws. The long sides of the frame act as columns to react the tension load of the straws. The side closest to the particle beam is made from carbon fiber reinforced plastic (CFRP) in order to minimize material. The side away

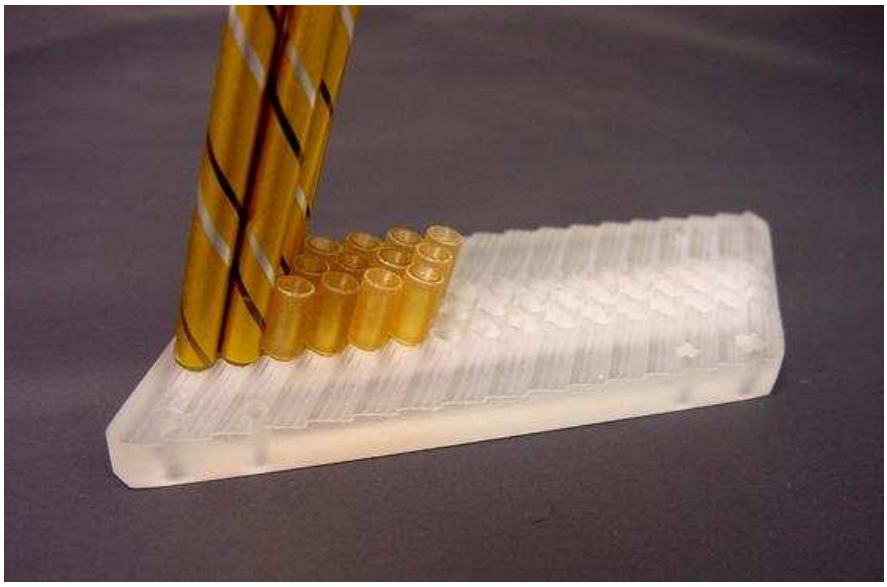

Figure 8.6: Endplate for stations 1 and 2

from the beam is made from aluminum. The frame also supports wires that are attached to the straws at intermediate locations along the length of the straws. These wires maintain the lateral alignment of the straws.

8.4.4 Half-view frame components

8.4.4.1 End Extrusions

The short sides of the half-view frame are made from aluminum extrusions. Aluminum extrusions were chosen because it is an economical method for producing the structural shape that fits the space constraints. The use of an extrusion also allow the cooling and gas to be supplied with passages incorporated into the structural shape (see Fig 8.8).

Prototype extrusions were obtained to verify that the required structural shape could be manufactured with internal passages. The prototype extrusions were also used to verify that the straightness and twist tolerances required for the half-view frames could be achieved. Inspections of sample extrusions confirm that the critical faces of the extrusion can be produced flat without requiring any additional fabrication operations. Not all extrusions are flat along the entire length but all have flat sections that can be used for the smaller stations. We expect that production extrusions will require inspection and sorting to select the appropriate section for the size of the half-view frame (see Fig 8.9).

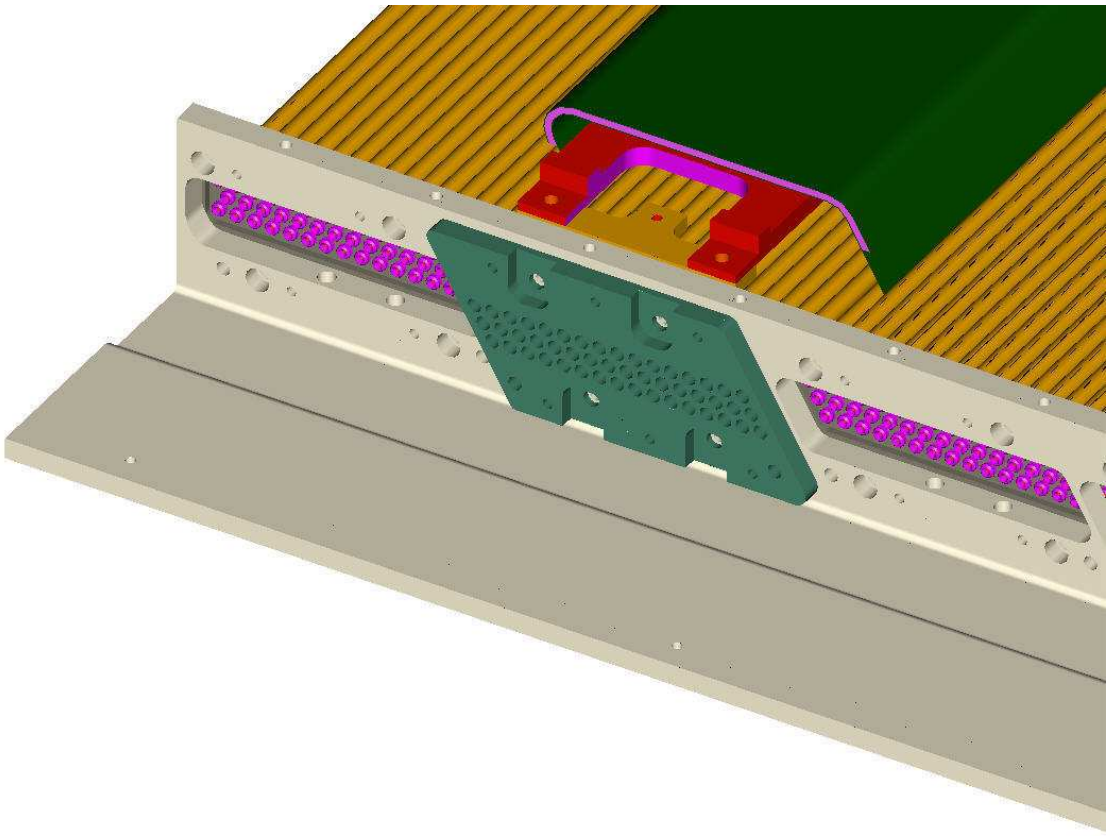

Figure 8.7: Detail of modules installed in half-view frame

8.4.4.2 Extrusion Machining

The ends of the half-view frame are made from segments of the extrusions that have been machined with the features for mounting the straw modules (see Fig 8.10). The features are a repeating pattern for each module. The features include a parallelogram shaped cutout for accessing the ends of the straws, pinholes for aligning the module, mounting holes for the module end-plate and wire tension plate (anode plate). In addition cross-drilled holes connect the gas supply passage of the extrusion with each module. Module-to-module spacing is controlled by the alignment pinholes of the machined extrusion and corresponding holes in the module end-plates.

8.4.4.3 Half-View Frame Deflection

The most significant load on the half-view frames is a result of the tension of the straws and anode wires. The tension load from each module is approximately 12 kg and that leads to a distributed load on the end extrusions of approximately 1.8 kg/cm. The deflections of the

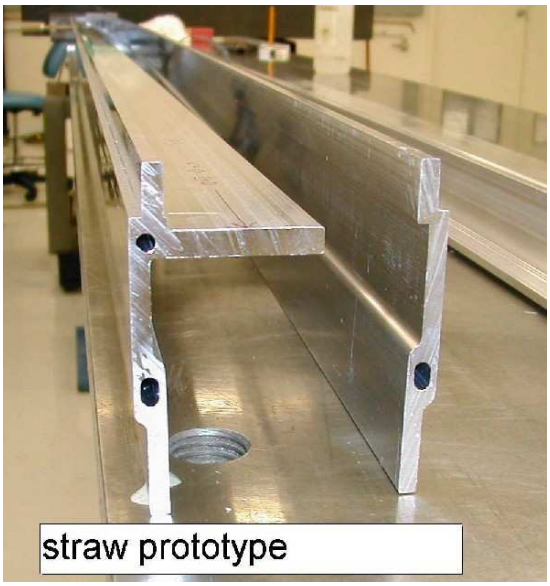

Figure 8.8: Extrusions for half-view frame

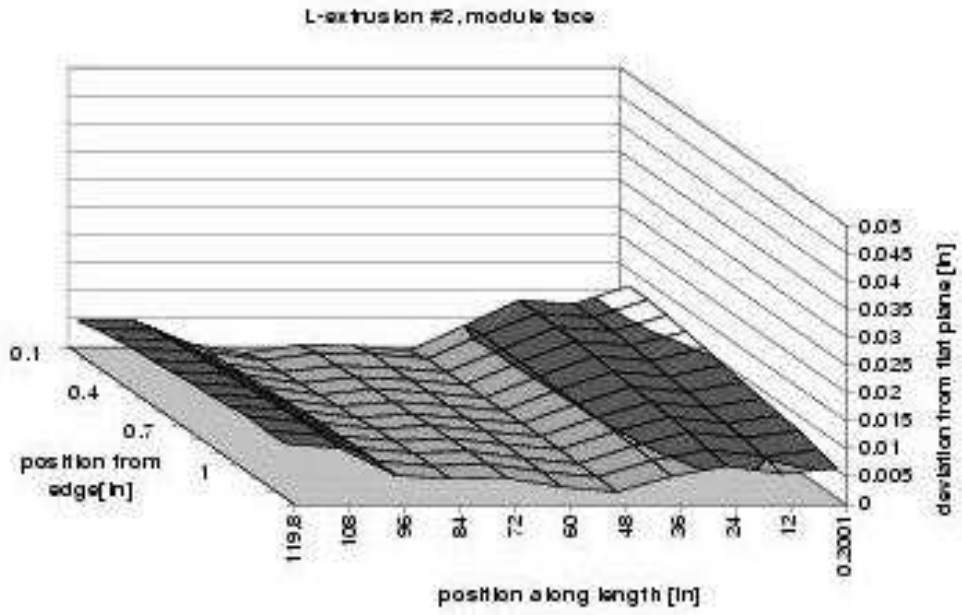

Figure 8.9: Flatness measurements of extrusions

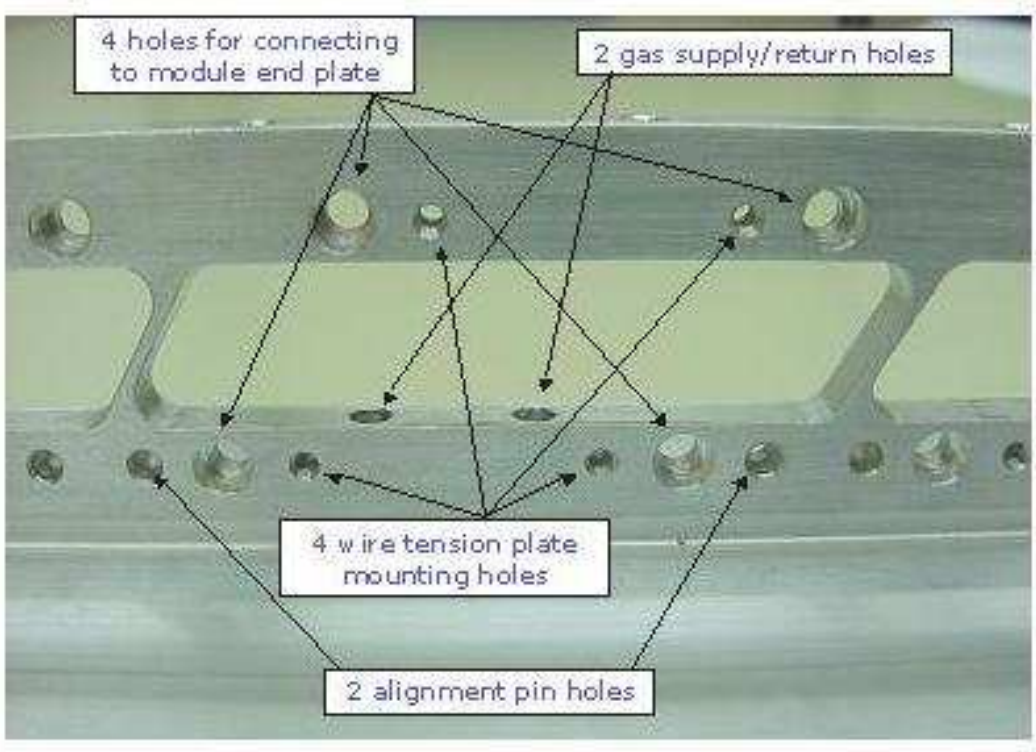

Figure 8.10: Extrusion showing machined holes

station 3 and station 6 half-view frames have been analyzed by finite element methods (see Fig 8.11).

The deflection at the middle of the chamber for station 6 was determined to be 0.5 mm. Straws tensioned to 200 g will stretch approximately 3.1 mm. Without compensation the tension in the straws in the middle of the half-view would be approximately 32% less than the tension in the straws near the ends. Thus some compensation method such as shims will likely be used to assure a more balanced tension among all the straws in a half-view. The anode wire for station 6 stretches approximately 5.8 mm and thus the wires near the middle would lose approximately 17% of their tension with the deflection of the extrusion. It has not been determined whether any compensation to maintain uniform wire tension is required.

8.4.4.4 Half-View Frame Strut

The load from the straw and wire tension on the extrusion is reacted by two struts that hold the extrusions apart. The design of the inner strut must be optimized so that it can reliably carry the compressive load with minimum material. The critical buckling load must have a sufficient safety factor to assure that any small imperfections in the shape or material of

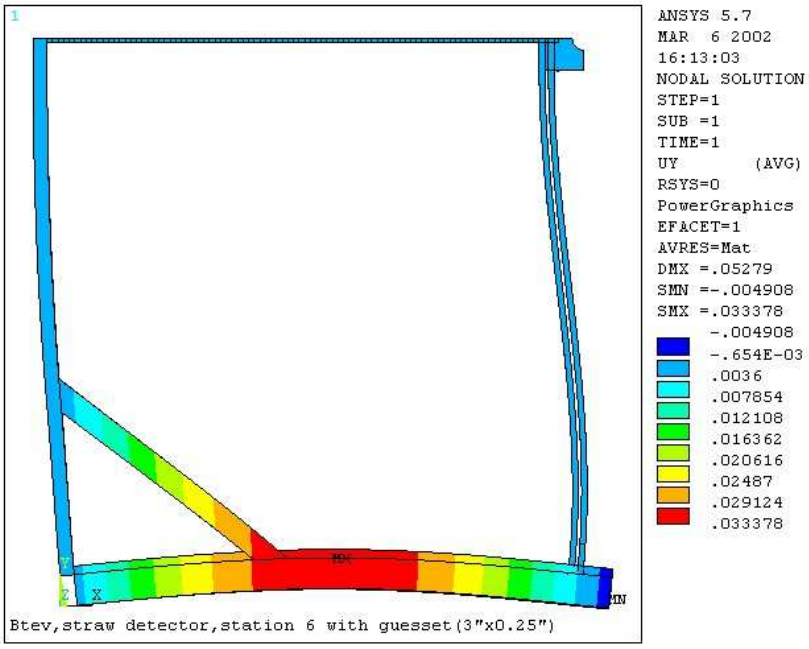

Figure 8.11: Finite element analysis of deflection of straw half-view frame

the strut do not lead to elastic buckling. Initially a strut design was investigated that would allow a standard module to be assembled after the strut was connected to the half-view frame. This assembly goal required a C-shaped strut that allowed a module to slide through the open side of the C. However, an open section like a C-shape is not torsionally stiff and is not able to react the tension of the straws without excessive twisting. Two alternate design options are being developed. The first option involves a closed section in the shape of a parallelogram so that one straw module can fit inside. The strut shape would allow a standard module to be slid inside before assembling the strut and module into the half- view frame. The second option is structurally more efficient but requires a special straw module that is assembled as part of the strut when the strut is constructed. This second option is similar to the module for the silicon support described in section 8.4.5.

Two prototype struts of the first option type were tested until failure under compressive loads. The prototypes are considerably shorter than the full length required and therefore test the section design with regard to local strength. The first prototype had a length of 10.5" and failed at 610 lbs. The second prototype with a slightly modified design was 14" long and failed at 916 lbs. The expected load at station 6 is 224 lbs. A cross section of the second prototype is shown in Fig. 8.12. More details can be found in a BTeV internal document[2].

Figure 8.12: Cross section of prototype carbon fiber strut

8.4.4.5 Center Manifold

To provide clearance for the beam pipe the inner-most module of each half-view frame is interrupted near the beam pipe. One side of the half- length module connects to the center manifold, which is attached to the middle of the half-view frame strut. The center manifold serves two functions. First it provides the tension connection between the two half-length manifolds to carry the load of the straws and anode wires from one half-length module to the other half-length module. Second, it provides the flow path for chamber gas from one half-length module to the other. The center manifold is shown in Fig. 8.13.

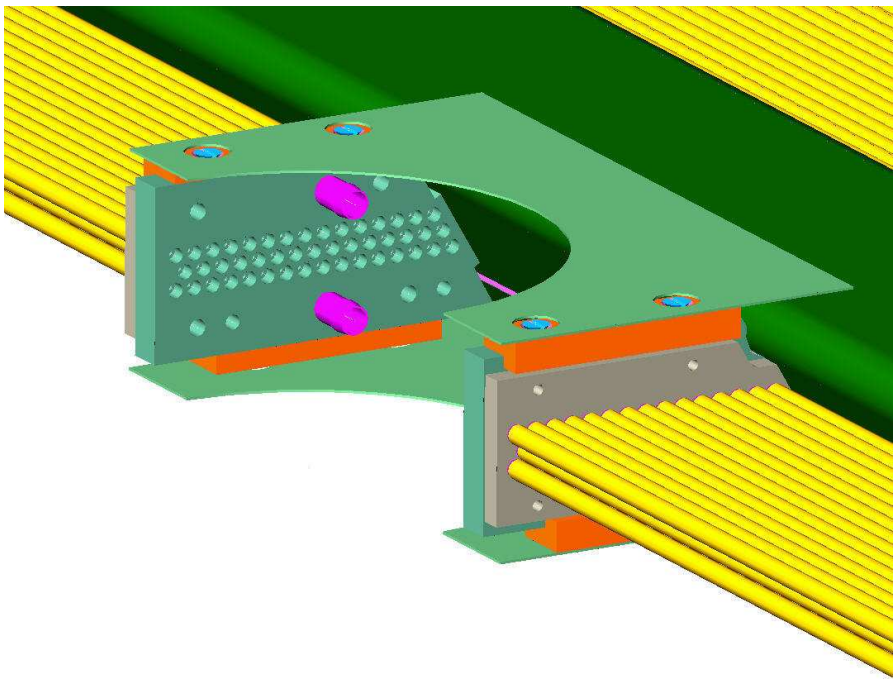

Figure 8.13: Carbon Fiber Center Manifold

8.4.5 Special Module for Forward Silicon support

A special module (MOX) that replaces the 2 modules that surround the beam-pipe in the X-view has been designed by INFN Frascati to support the forward silicon planes at each station. It is shown in Fig. 8.14. The straws in this module are embedded in rohacell so they are kept straight without needing to be under tension. The rohacell is surrounded by a carbon fiber shell. A carbon fiber disk to support the forward silicon is attached to the module shell.

Fig. 8.15 shows a detail of this module around the beam-pipe. The straw tubes are glued to the end plate as done for the other modules. However the glue must meet less stringent requirements than the glue used on other modules, since in this part of the detector neither electrical conduction (wire is deadened few centimeters from the endplate on the beam side to limit rate) nor mechanical tension on the straws is required. The main function of this glue is therefore that one of sealing, and a wide variety of options are available.

Since no tension is applied to the straws of the M0X, this end plate can be made of very light material such as polyimide, etc.

Wires are pinned to the anode pinning plate. In Fig. 8.15 the anode pinning plate is cut out so that it is possible to see the straw endplate described above. The anode pinning plate is designed to withstand the tension of 98 wires at 50g per wire. This plate has to be gas tight. The gas flowing from the upper half of the M0X is collected in the gap between the two plates described above, will flow to the lower gas gap through low-Z tubing, and then to the lower half of M0X.

The total material in the assembly is expected to be approximately 0.7% of a radiation length. Initial studies of the deformation of the module under the weight of the silicon strip assembly indicate that this is acceptable. A more detailed finite element analysis will be done soon.

Deformations of the special module will be monitored in real-time by use of Fiber Bragg Grating(FBG) sensors[3]. FBG sensors will be embedded in the carbon fiber structure and will provide monitoring of straws and silicon detector positions[4]. The FBG sensors will also be adopted for accurate monitoring of the Pixel detector suporting structure and will thus provide a highly reliable monitoring technique for the overall geometry of the forward tracking detectors.

8.4.6 Station 7

Station 7 of the Straw Detector will be constructed in super-modules to enable it to be installed around the beam-pipe in the restricted space between the RICH and the ECAL. Each view is composed of 8 super-modules assembled together by a light-weight channel type outer frame. Each super-module is approximately 400 cm x5 cm x43 cm, with an aluminum extrusion at each end for mounting 6 modules. The super-module shell frame is a bridge that connects the two aluminum extrusions and is made of CFRP with a thickness of 0.5 mm. Each super-module weighs about 10 lbs. and can be handled individually for installation.

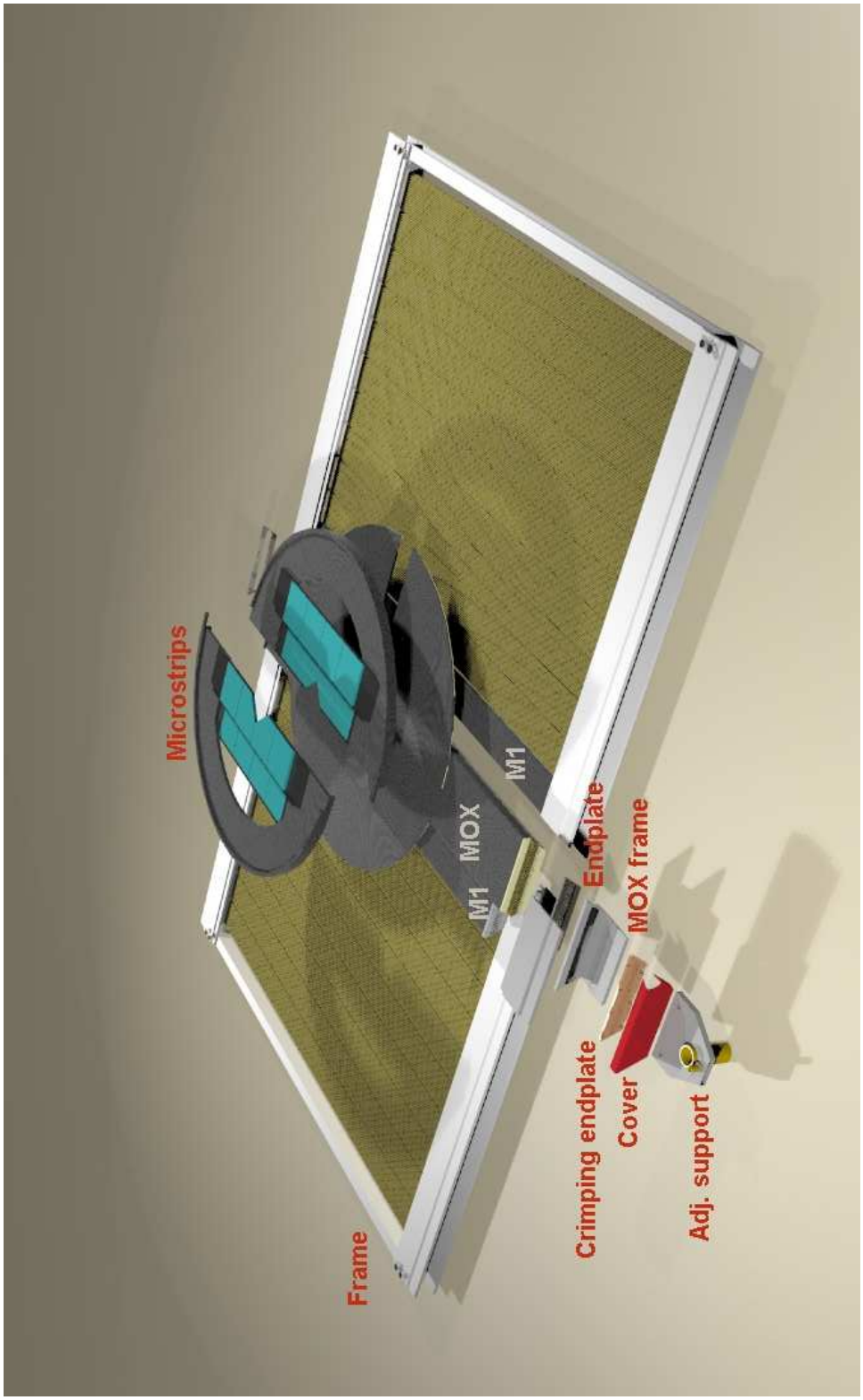

Figure 8.14: Special module to support forward silicon

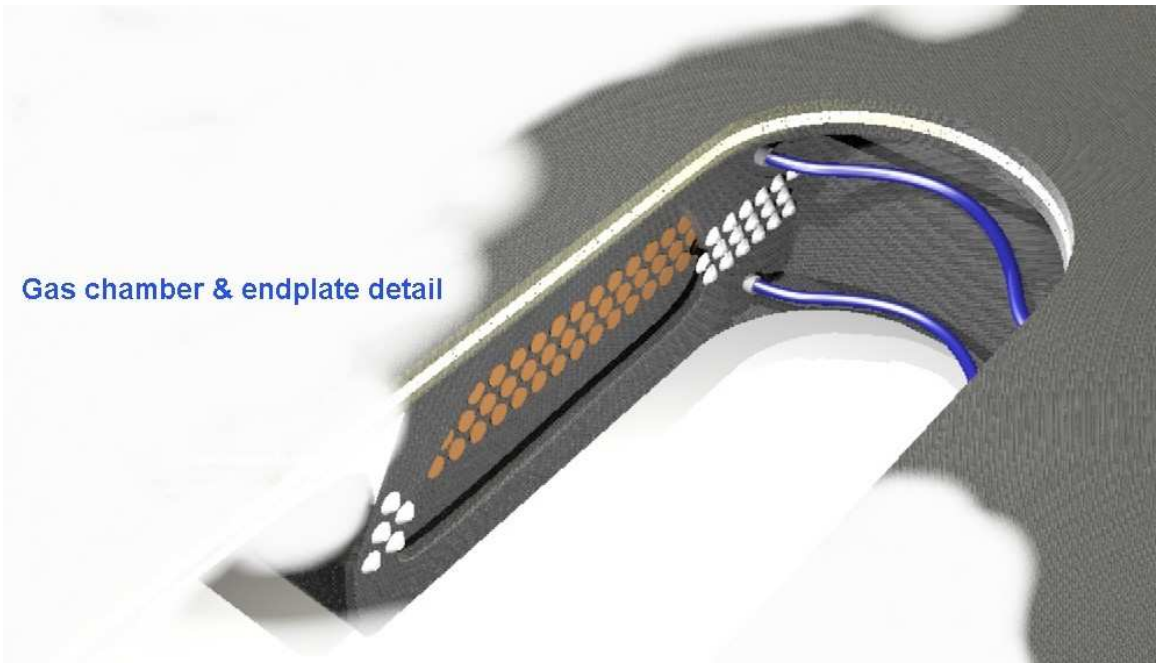

Figure 8.15: Detail of the MOX around the beam-pipe

In addition to connecting the two aluminum extrusions, the super-module must support a force of about 12 Kg/module due to the tension in the straws and wires.

Four fiber sheets form a hollow tube type frame, as shown in Fig 8.16. The two faces of the major plane of the frame have 10 holes 28 cm in diameter to provide access to the straws and to reduce the weight of the frame.

To understand the mechanical behavior of the super-module frame, the engineering group developed finite element models to simulate the behavior of the frame under various working conditions. It was found that the maximum deflection in the major plane of the frame is about 0.0076 mm and the maximum deflection in the perpendicular direction is 0.0069 mm. Using the Linear Buckling method it was found that the super-module will not fail until the axial load increases from 12 Kg/module to 86 Kg/module.

8.4.7 Beam-Line Supports

The straw half-views for stations 1-6 will be assembled into full stations as described in section 8.8.3. Stations 1-3 will be mounted directly to the dipole magnet at four corners with a kinematic support system. Station 4 will be attached to the magnet flux plate. Fig 8.17 shows the support mechanism for Station 3.

For Station 7 each view will be mounted independently. The supports will be cantilevered off the toroid magnets, see Fig 8.18.

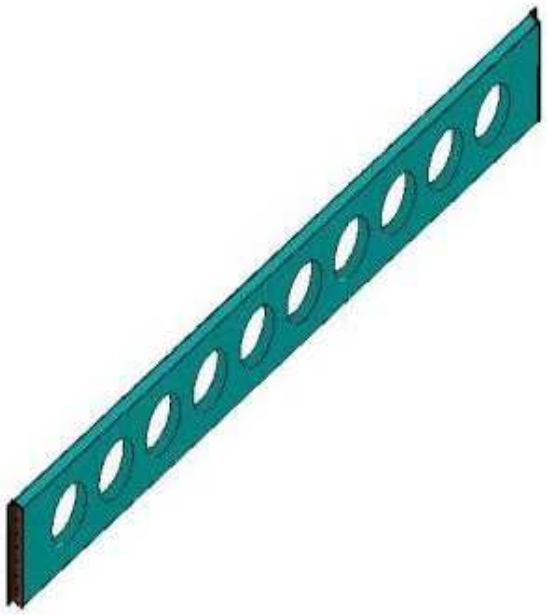

Figure 8.16: Station 7 super-module

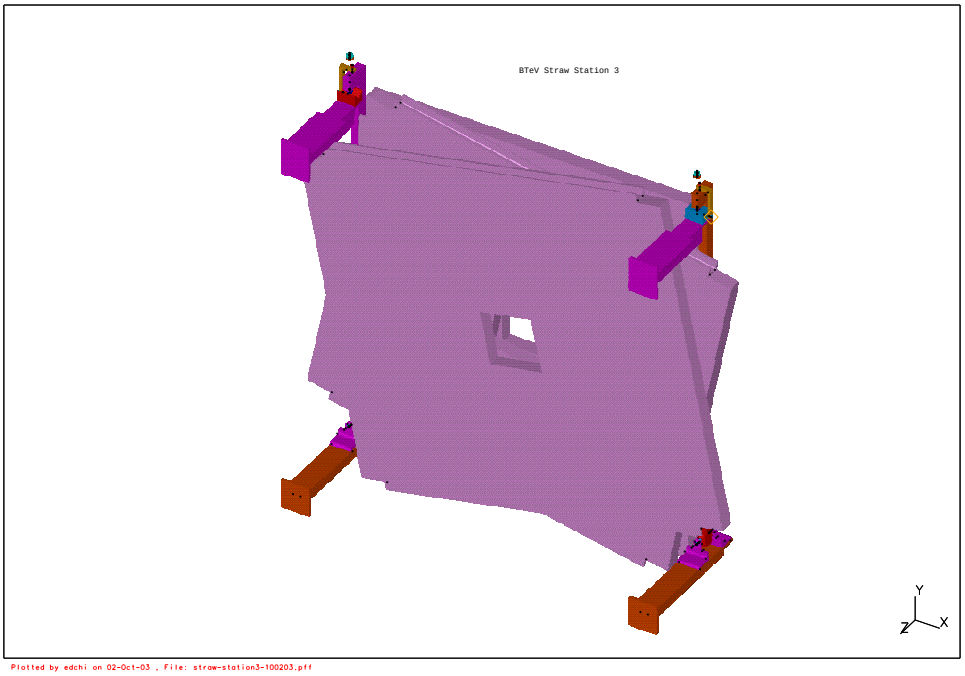

Figure 8.17: Station 3 support structure

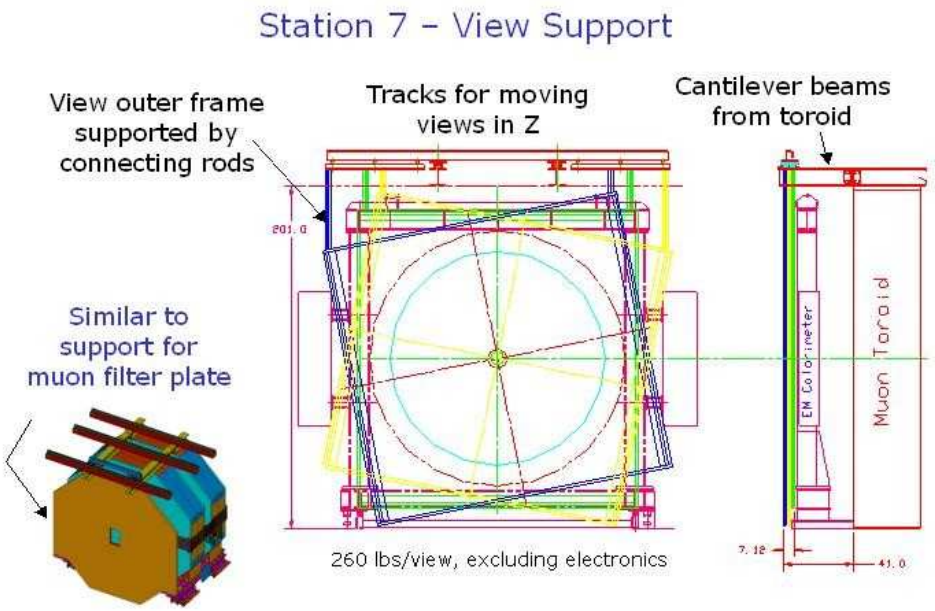

Figure 8.18: Station 7 support structure

Table 8.2: Material budget of Straw Chamber

Material	Fraction of X_0/station
Straw walls (kapton + Aluminum)	0.50%
Wires	0.13%
Gas	0.02%
Twisters	0.04%
Carbon Fiber struts	0.09%
Mylar windows	0.15%
Total	0.93%

8.4.8 Material Budget

The total amount of material per station is about 0.9% of a radiation length averaged over the active region outside the central gas manifold and inside the frame. The largest fraction comes from the kapton. Details are shown in Table 8.2. The material in the center gas manifold region is the manifold itself plus tension plates to hold the wires. The average material in this region is about 3% X_0.

8.5 Calibration, Monitoring and Control Systems

8.5.1 Straw Gas System

For BTeV straw cells we plan to determine the gas mixture which optimizes drift time resolution, efficiency, and stability of operation.

Closely associated with the choice of gas mixture will be the determination of optimal gas gain at which to operate the detector. Higher values of gas gain are known to introduce space-charge effects which can lead to significant non-linearities in the straw response. The probability that self-limiting streamer discharges occur rises quickly with gas gain. This in turn leads to an overloading of the front-end electronics and introduces deadtime in the amplifier/shaper/discriminator circuitry. The baseline choice of gas is an 80:20 mixture of Argon-CO_2. The drift speed is adequate, being about 50 μm/ns giving a maximum drift time of about 40 ns for a 4 mm diameter straw. An advantage of Argon-CO_2 is that it does not have deposits due to polymerization which occurs with hydrocarbon gases in a high rate environment. Aging in Argon-CO_2 is thought to be mostly due to contamination of the gas. To minimize this we will use stainless steel tubing and test all gas before it is used in the straw chambers. It is particularly important to remove all trace of sulfur compounds if we use copper cathodes. We plan to continuously monitor the gas gain, drift speed and gas composition.

The design of the BTeV straw chambers from a gas perspective has been evaluated, and a system to supply these chambers has been designed. The flow distribution was studied with a three-dimensional ANSYS diffusion finite element model. The detailed results are given in a BTeV internal document[5]. Within a module of 48 straws, the flow distribution varies about 15% which is adequate. The flow between modules will be balanced by placing a restriction at the inlet of each straw module, which can be accomplished by reducing the diameter of the two flow paths feeding each module, or placing a sintered metal orifice in the flow path. The gas flow distribution to an 8-module half-view is shown in Fig 8.19. The gas supply system is based upon the E815 Argon-Ethane flammable gas mixing system. In order to maintain the straws at a stable humidity, each straw half-view will have mylar windows within which we will flow dry nitrogen.

8.5.1.1 Gas Monitoring

We intend to monitor the straw chamber fill gas for gas gain determination, pollutant level and drift velocity determination.

Accurate knowledge of the gas gain is necessary to set a working voltage for the straw anodes that optimizes overall straw performance (i.e., optimizes detection efficiency and minimizes likelihood of after pulsing and streamer generation). We intend to measure the gas gain of the straw fill gas by irradiating a small number of 4 mm diameter straws with an ^{55}Fe source and then pulse height analyzing the resulting straw output signal to monitor the peak position corresponding to an energy deposition of 5.9 keV. Depending on the magnitude of the gas gain variations, the high voltage applied to the straw anodes can then be altered in

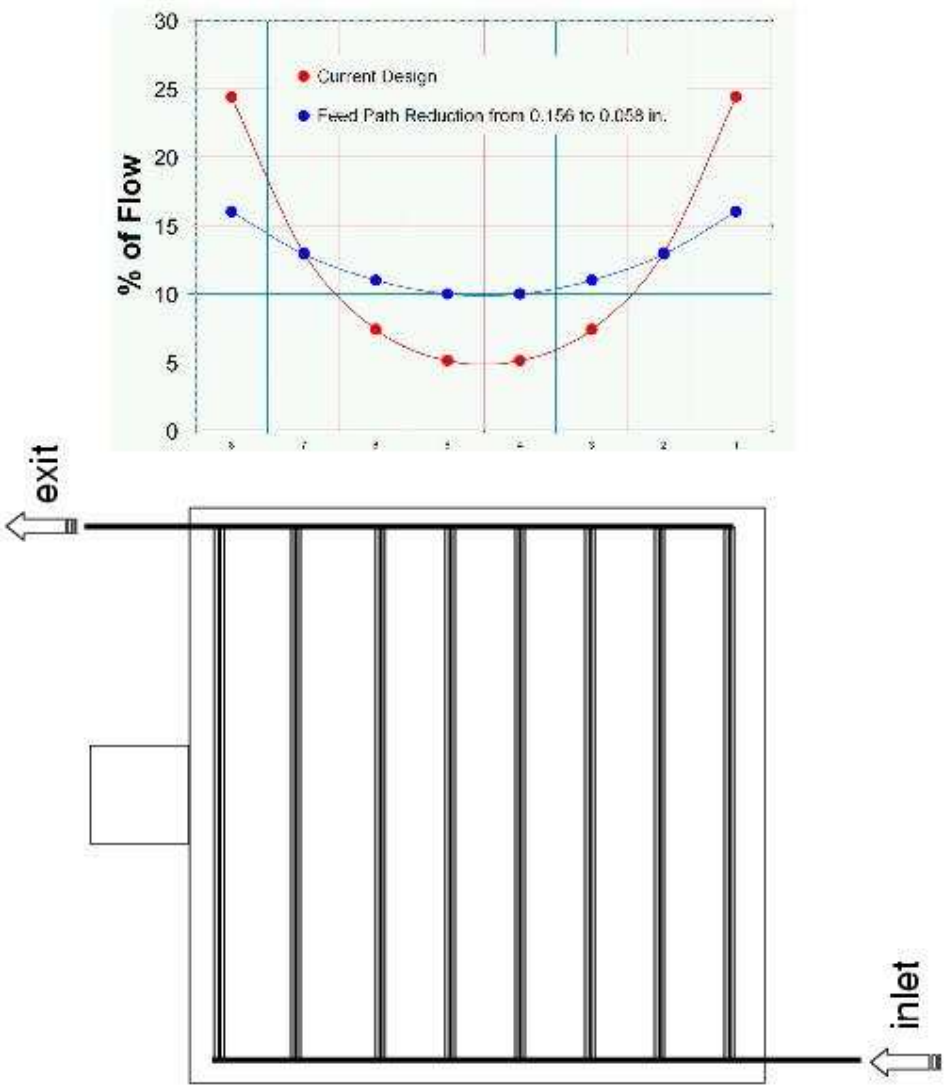

Figure 8.19: Gas Flow

a sensible fashion. The monitoring straw tubes will be built from hardware used to construct the actual tracking chamber and the readout electronics will be non-exotic.

The pollutant level of the straw chamber fill gas will be measured by feeding the exhaust gas from the straw stations into a mass spectrometer/gas chromatograph. (The fill gas will also be qualified before it is admitted to the chambers.) This diagnostic information will be coupled with the drift velocity monitoring measurement to help maximize tracker performance and to help diagnose problems like low or time-dependent detection efficiency. Precise details of the system are not yet fixed since the requisite pollutant sensitivity and the full spectrum of likely pollutants depend on key details like the choice of fill gas, still undecided at this point.

Prototype work has started on developing a special monitoring chamber that would measure the drift velocity of the straw fill gas. Accurate knowledge of the electronic drift speed is required for optimal straw tracking resolution. Light from a N_2 laser is directed into a special box-shaped chamber that would measure the electron drift speed in a uniform electric field. The laser permits the straightforward generation of a strobe to mark the start of the electrons' drift and the chamber would be filled with the exhaust gas from the straw stations, ensuring the test chamber uses the same gas as the actual tracking chambers. Preliminary estimates show that a fractional accuracy of 1% in the electron drift speed is practicable, consistent with our requirements. The exact number of test chambers to be used is not yet fixed.

8.5.2 Water Cooling System

The Straw Detector frames are cooled by flowing water through the aluminum extrusions. Each U-shaped extrusion has 2 cooling channels.

The cooling system will have two 50 gpm water pumps outside the collision hall. Normally one pump will be running and the other will serve as a backup. Above the pumps will be a water expansion tank to supply a positive pressure to the pumps and to vent air from the system. The cooling system will be a closed loop with no copper or copper alloy materials to avoid galvanic corrosion in the aluminum extrusions. The return flow will pass through a heat exchanger in which chilled water will flow to keep the straw cooling water at the desired temperature. The straw chambers will operate at the ambient temperature of the collision hall.

In the collision hall there will be one main supply and one main return water header on each side of the detector. The cooling channels in the aluminum extrusions will connect to these headers. Each half station will have a manual valve to balance the flow between stations.

The heat load, flow rates and temperature differences are shown in Table 8.3.

Table 8.3: Heat Load and Flow rates in Straw Detector Cooling System

Station	Power/station (W)	Flow rate/station for 0.3C temp rise (L/min)	Pressure drop in cooling channel (Bars)	Temp difference Extrusion-water (C)
1	184	9.7	0.005	0.57
2	276	13.7	0.013	0.45
3	415	21.6	0.042	0.35
4	599	30.6	0.108	0.27
5	691	35.1	0.156	0.24
6	783	39.6	0.217	0.22

8.5.3 Environmental Control and Monitoring

In order to keep the straws straight it is necessary to keep them from sagging due to changes in temperature and humidity. Relative humidity will be kept close to 0% by flowing dry nitrogen in a closed volume around each half-view. We require that the temperature in the C0 hall to be stable to $\pm 1^oC$, though there may be several degrees temperature difference between the top and bottom of the hall. The frames of the straw half-views will have the temperature controlled by flowing chilled water through them.

Each half-view will have a temperature and humidity sensor and the high voltage will be turned off if either is out a pre-determined acceptable range. Sensirion manufactures a compact, inexpensive line of chips (SHTxx) that would satisfy our requirements for temperature and humidity sensors.

8.6 Performance

8.6.1 Resolution

The momentum resolution as a function of track momentum is shown in Fig 8.20. We expect to have a single straw position resolution of $150\mu m$. We have constructed a two module prototype detector which is currently in the test beam. Fig. 8.21 shows a test beam particle passing through the straw prototype and wire chambers upstream and downstream. We have not yet analysed the test beam data.

8.6.2 Occupancy and Tracking efficiency

If BTeV runs with a 396 nsec bunch spacing, the occupancies in the the Straw detector will be about three times higher than was expected at the time of the BTeV proposal. This leads us to consider whether it would be advantageous to increase the size of the forward silicon strip planes ie. increase the size of the "dead" region of the straw detector. There will be a

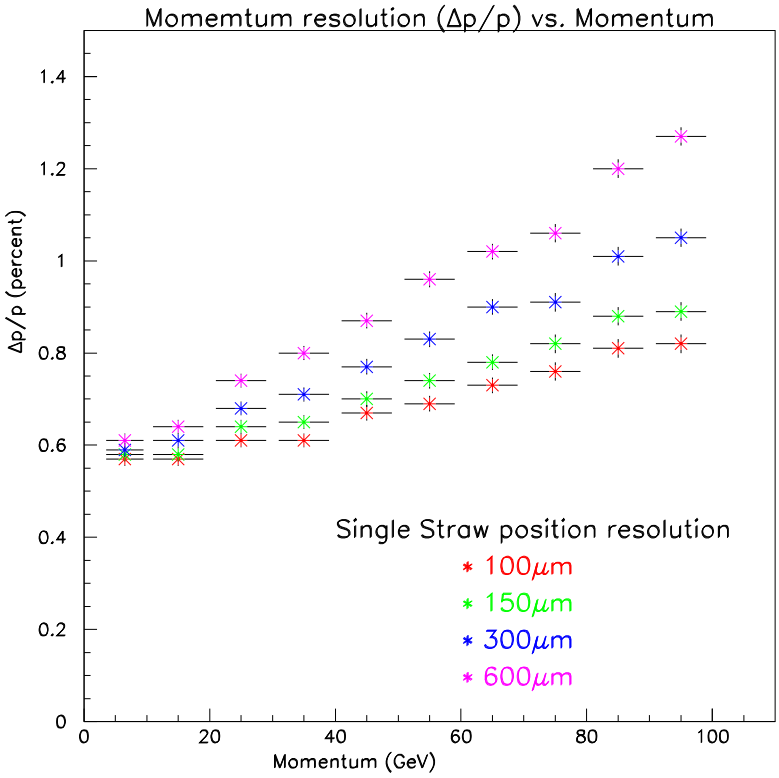

Figure 8.20: Momentum resolution as a function of track momentum, for tracks that pass through at least 6 forward tracking stations

compromise between the reduced occupancy and the increased material which leads to more multiple scattering.

The baseline design has silicon planes 27cm x 27cm. We have studied occupancies and tracking efficiencies comparing this baseline size with an alternative design having silicon planes 40cm x 40cm.

Figure 8.22 shows the occupancy of the Straw detector at Station 6 for a B interaction accompanied by a varying number of minimum bias interactions for the two different size silicon planes. The occupancy in the center of the detector drops by about 25% with the larger silicon planes.

The tracking efficiency was studied for two cases; firstly for tracks that have hits in at least 4 pixel stations so that a seed track can be found in the pixel region and projected downstream to the forward tracking stations, and secondly for tracks such as those from the decay of K_ss or Λ^0s that do not have enough pixel hits to seed the track in the pixel region. The efficiency for pixel seeded tracks with momentum greater than 3 GeV and with hits in

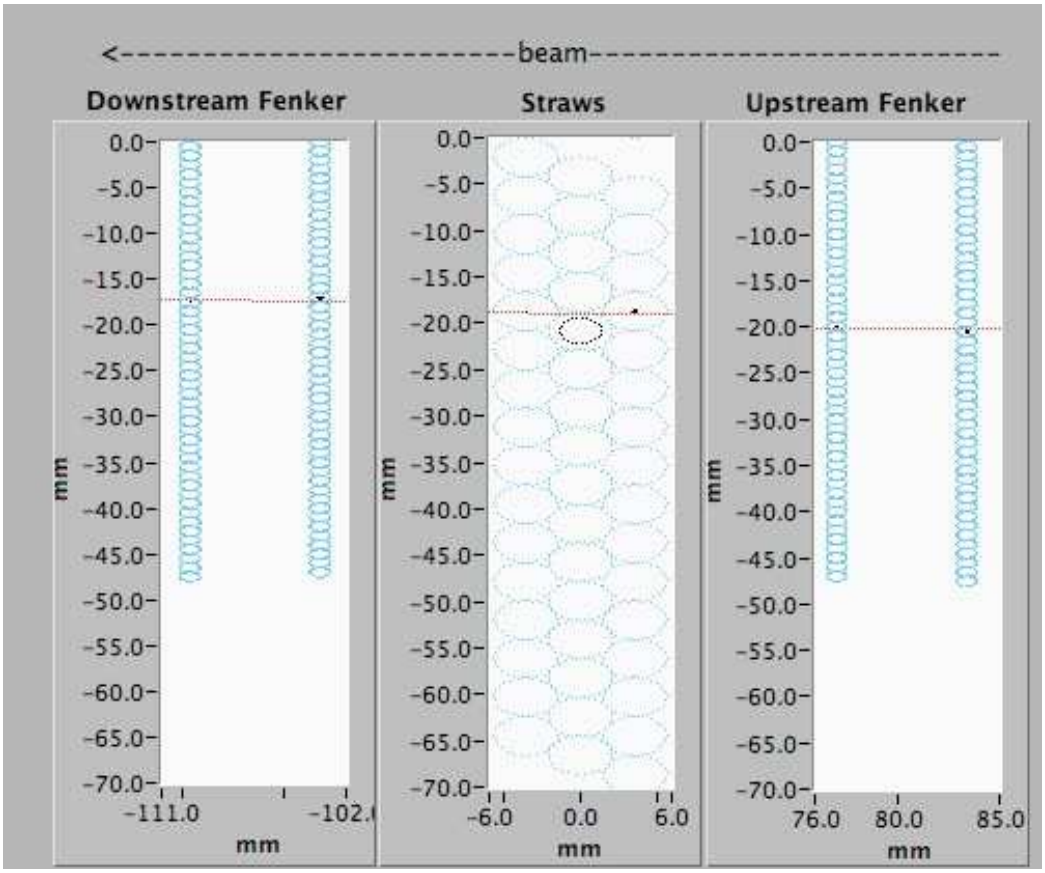

Figure 8.21: Track from test beam passing through straw prototype detector and wire chambers

at least four downstream stations drops from 98% at 2 interactions/crossing to 95% at 9 interactions/crossing but there is no improvement with larger silicon planes.

For tracks without pixel hits we also see no improvement in efficiency with larger silicon planes, but there is a reduction in the number of ghost tracks. We believe that increasing the size of the silicon planes does not give enough improvement in performance to justify the increase in cost.

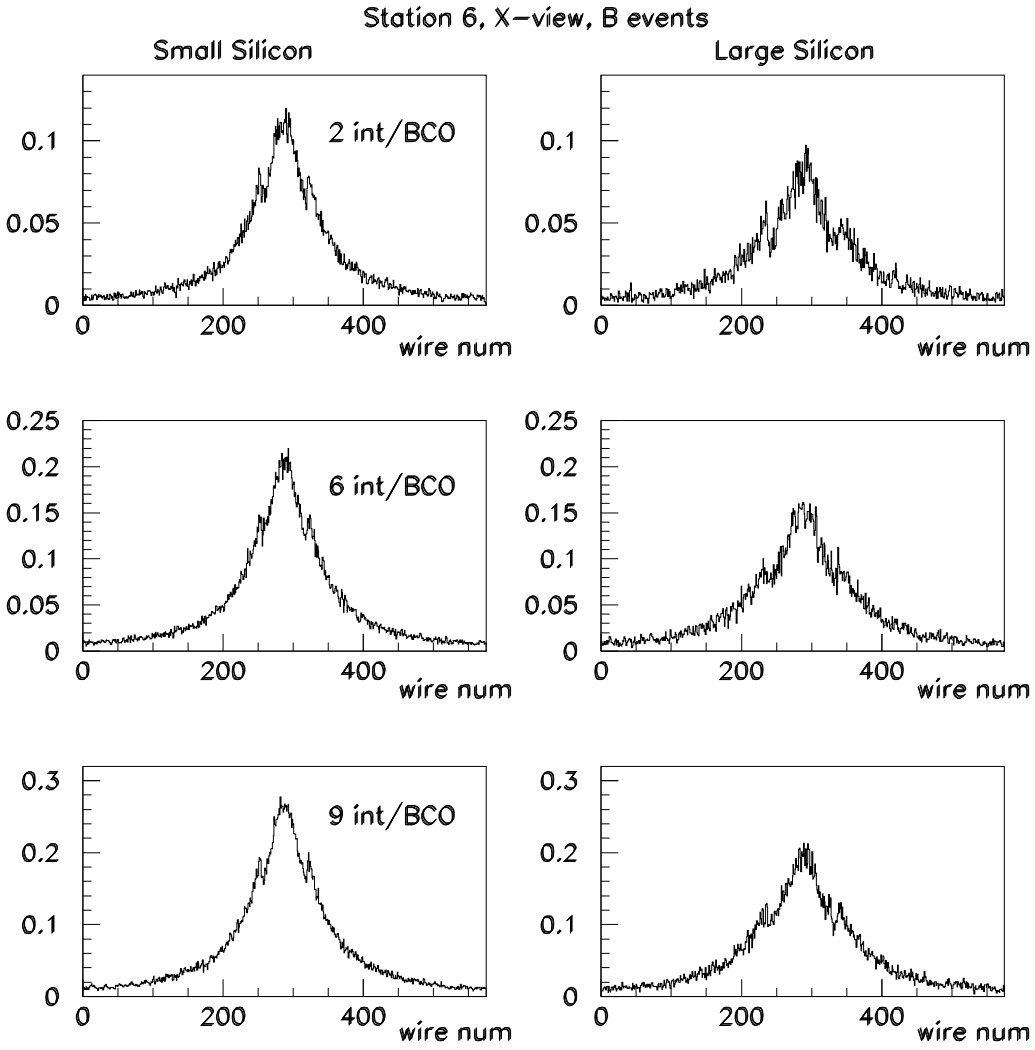

Figure 8.22: Occupancy of Straw Station 6, X-view for a B interaction plus 2,6 or 9 minimum bias interactions. Left side: Dead area 27x27 cm; Right side: dead area 40x40 cm

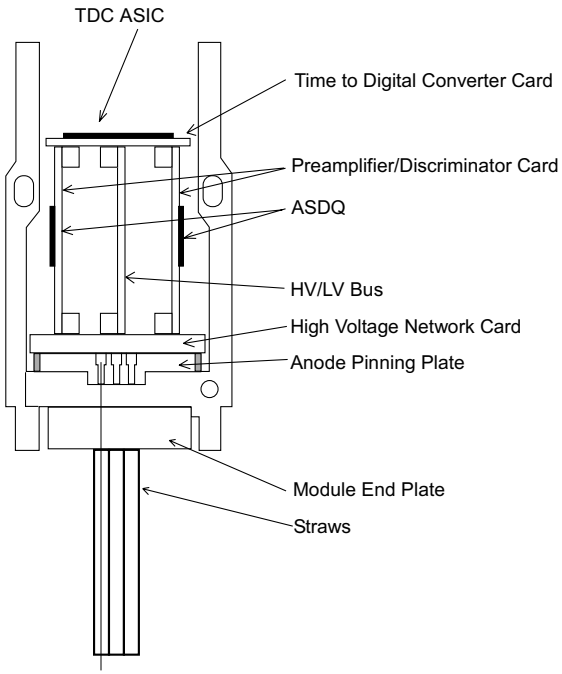

Figure 8.23: Schematic view of Electronics Packaging inside Straw Frame. The ASDQ's are located on the side nearest the channel to facilitate cooling (liquid cooling channels are located in the channel sides).

8.7 Front-End Electronics

8.7.1 Introduction

The Straw Front-End Electronics is composed of 6 blocks. They are the Anode Pinning Plate, the High Voltage Network Card , the High Voltage/Low Voltage Bus, the Preamplifier/Discriminator Card, the Time to Digital Converter Card, and the daughter card of the Data Combiner Board. The following description is based upon the modularity of the straw detector, with a single module containing 48 straws. Each straw will be electrically divided by an insulating-glass bead. With this setup, we read out both sides of a straw. Fig 8.23 shows a conceptual view on how the electronics are architecturally arranged in the channel of a straw frame.

8.7.2 Anode Pinning Plate (APP)

The APP (Fig 8.24) is used to keep the 25 μm diameter, gold-plated tungsten anode wire at a nominal tension of 50 grams. It is the same shape as the module end-plate, made of Noryl plastic, with brass eyelets inserted into the 48 holes. During the wire stringing process, the anode wire is threaded through the eyelets, and captured by a tapered brass pin, which

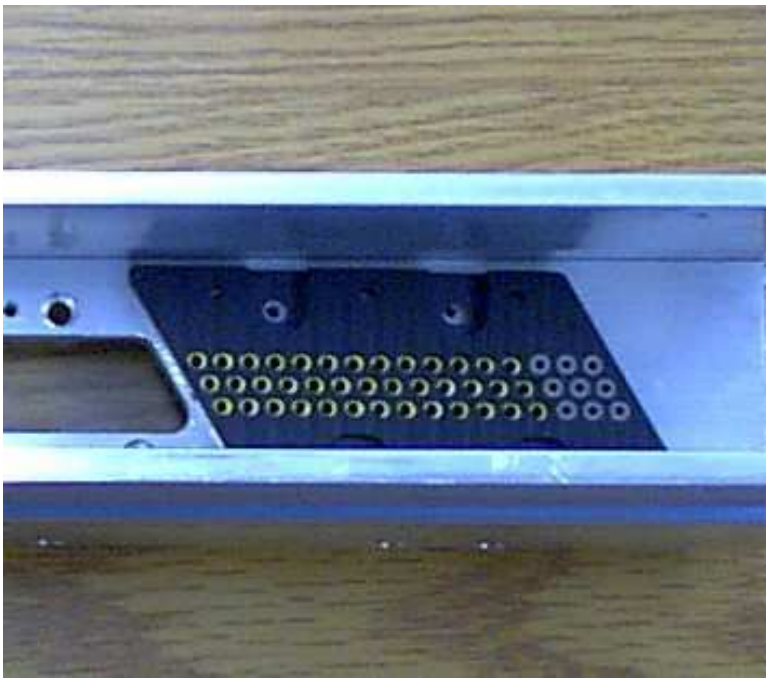

Figure 8.24: Anode Pinning Block shown in Straw Frame. The brass eyelets can be seen in the majority of the holes, while the conductive elastomer (gray color) can be seen in the right three rows.

just fits into the inner diameter of the brass eyelet. We have been monitoring the holding capability of this system for over a year with no apparent problem in its ability to hold the wire tension.

The depth of the holes in the APP insures that the heads of the brass pins are significantly lower than the APP top surface. In order to make electrical contact to the anode wire, conductive elastomer inserts (cylindrical in shape with a coaxial hole to clear the head of the brass pin) are inserted over the brass pin and into the APP hole. Electrical contact is made between the upper face of the brass eyelet and the lower face of the conductive elastomer. The conductive elastomer is a snug fit into the hole. The height of the conductive elastomer is just short of reaching the top of the hole. Contact with this surface is made by conducting pads on the High Voltage Network Card.

8.7.3 High Voltage Network Card (HVNC)

The High Voltage Network Card is the means to deliver the high voltage to the anode, and to bring the straw signal to the Preamplifier/Discriminator Card. The Straw Detector is operated with a positive high voltage on the anode and the straw cathode at ground. This is done for two reasons: firstly for safety as the cathodes at negative high voltage might pose a safety hazard during construction and testing, and secondly because we want the capability

to disconnect the high voltage from a single straw in case of breakdown. Since the straw cathodes are closed packed, this might be quite difficult to achieve. With the high voltage on the anode, it can be simply disconnected from the HV by cutting a trace on the HVNC.

Due to the close packing of the straws, the desire to disable a single wire, and the close proximity of high voltage traces to signal traces, the printed circuit board layout demands a multi-layer board. The side of the HVNC closest to the APP has 48 pads which protrude enough to make contact with the 48 conductive elastomers of the APP. Each of the protruding pads has a via to the inner board layer. In this layer the traces are routed to the top of the HVNC in a manner to enable the layout of the pads for the load resistors, blocking capacitors, and connectors which carry the straw signals to two 24-channel Preamp/Discriminator boards.

Under normal running operations, the case of a broken anode wire would be handled by turning off the HV to the entire 48 channel module. At a later date, when access time to the detector permits, the trace to the load resistors of the broken channel would be cut to disable the wire. Under extraordinary conditions, an attempt to fix a straw channel might be attempted, but most likely only if the particular straw detector has been removed from the experimental hall.

8.7.4 High Voltage/Low Voltage Bus (HVLVB)

The HVLVB is a single printed circuit board that we will use to bus the high and low voltages to all the modules in a straw half-view frame. The HVLVB connects the high voltage through pins to the HVNC, and low voltage to the TDCC card. Our base plans use a single high voltage channel per straw module. If a wire breaks in a single module, the HV will be turned off for the entire module. It might be more effective to arrange the HV so that a single channel supplies the HV for a single plane in 3 adjacent modules. In that way, a single broken wire will not completely disable the tracking over an entire 3-plane module of straws. The final arrangement of the HV bus will be decided after further study of other possible failure modes of the straw system. However either arrangement should be easily handled in the HVLVB. Both sides of the Straw Chamber will have a HVLVB. At this time we intend that the HV in any one straw will originate from a single HV channel supply. This is to insure that the central anode insulating glass bead will not have to hold off a possible large HV difference caused by turn-on or turn-off lag in the power supplies.

8.7.5 Preamplifier/Discriminator Card (PDC)

We are currently planning to use the ASDQ preamplifier/discriminator chip in our PDC card. The ASDQ was developed at the University of Pennsylvania for the CDF Detector at Fermilab[6]. While we do not plan to use the "Q" feature of the ASDQ (a charge measurement) for the straw detector, nevertheless the chip itself adequately meets our requirements of low threshold and robustness. Each PDC will hold three 8-channel ASDQ's, so that each straw module will require two PDC's per side, for a total of four PDC's per straw module.

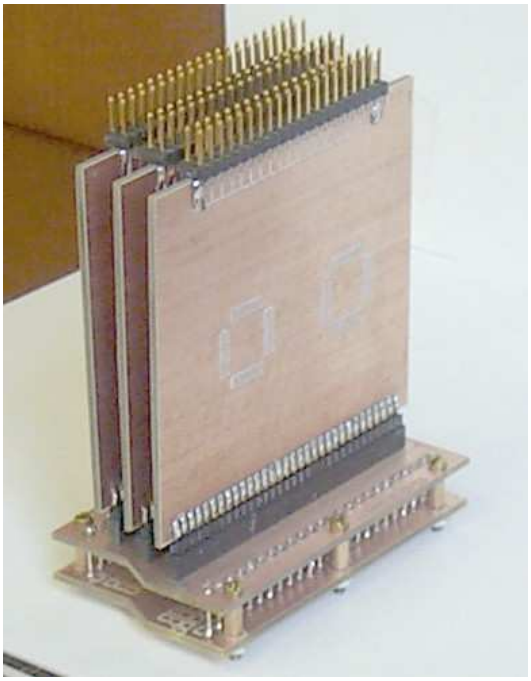

Figure 8.25: Prototype of Preamp/Discriminator Card and High Voltage Network Card (H.Powell and W. Stephens, UVa). This shows a prototype version of the 16 channel PDC(2 ASDQ chips/PDC) mounted on a prototype HVNC.

The two PDC's plug into the HVNC with the ASDQ inputs being coupled to the low voltage side of the blocking capacitor. The differential outputs of the ASDQ are sent to the output connector on the PDC. As currently planned, the two PDC's are plugged into the HVNC at a 90 degree angle, similar to that for a prototype 16 channel PDC as shown in Fig 8.25. The Time-to-Digital Converter card straddles the output connectors of the two PDCs. While we are constructing the detector, the Time-to-Digital Converter card will be replaced by a simple connector card so that we will have access to the discriminator outputs for testing and QC. All control and power of the PDC will be supplied from the TDCC card connector.

8.7.6 Time to Digital Converter Card (TDCC)

The TDCC card is the control card for the entire module front-end electronics. It receives the clock and control signals from the Data Acquisition System, supplies thresholds for the ASDQ's on the PDC, and performs a time analysis on the ASDQ Discriminator outputs. It is responsible for sending data on every beam crossing, and also controls the calibration of the ASDQ's and the Time to Digital Converter. A strong motivation of the Straw Electronics System design is to minimize the cable plant. The Straw Detectors are large flat detectors. They are relatively thin in order to minimize the longitudinal footprint of the BTeV Detector. This makes it difficult to mechanically support a large number of cables. These cables include

signal, control, high voltage and low voltage cables. The high voltage and low voltage will be distributed internally by a bus to the local module. Due to constraints of available space and conflicts with other detectors, the cabling is planned to run inside of the electronics channel in the straw frame and exit at the outer edge. The design for the TDCC and its component ASIC chips is specifically driven to minimize the number of input control and output data cables. We expect to use two input twisted pair lines and two output twisted pairs line per module side.

8.7.7 TDC ASIC

We are undertaking the development of a 48 channel ASIC which will supply the functionality of a Time to Digital Converter to measure the drift time of the tracks in the straws, and at the same time will also give us the interface into the BTeV DAQ system. These two functions will be discussed separately as the "TDC" and the "I/O Interface". There will be one TDC ASIC per TDC card.

8.7.7.1 TDC Requirements

- Time resolution/range: The charged particle tracking requirement for the straw detector is to measure a track position with an rms precision of 150 μm per straw. For the typical gases and applied high voltage that we plan to use, the electron drift velocity is about 50 μm/ns. Therefore the 150 μm precision equates to a timing spread of 3ns rms. For other reasons (which will be discussed in the "I/O Interface section"), we have decided that the time resolution of the TDC is adequately handled by a bit size of 1.56 ns. This bit size itself has a nominal rms spread of 0.5ns. This adds only a negligible amount to the uncertainty of our time measurement. The standard straw size for the BTeV Straw detector is 4mm diameter, so the maximum drift time for an electron is $\sim$40 ns. In certain cases we are considering 8 mm diameter straws (when the occupancy drops to a very low level), and so here the maximum drift time is on the order of 80$\sim$100 ns (depending exactly on how we arrange the drift field). In the 4mm case, the entire drift time is covered by a 5 bit TDC (50ns), while the 8mm case is covered by a 6 bit TDC. We are considering a fine/coarse TDC setting which would allow us to double the TDC range, simply to ease the initial setup of the system during the commissioning phase of the experiment. This can be accomplished by either halving the clock speed or alternatively simply doubling the total number of bits by delaying the reception of the timeout pulse.

- Single hit Capability: The straw detector is operated under conditions where the time between beam crossings is longer than the maximum drift times of a track within the straw. Any single track may give an analog signal into the discriminator ranging from 20 ns (track impact parameter near straw edge) up to a signal which is as long as the entire drift time (the case where a track has zero impact parameter to the anode wire, and clusters drift in over the entire radius of the straw). There is no intrinsic way to

separate out two tracks from the case of multiple electron clusters from a single track. This means that multi-hit capability is unnecessary. Because a single track will give rise to multiple hits, and since we are only interested in the earliest hit, the TDC will be operated in "start" mode. Only the earliest hit will be recorded by the TDC.

- Readout Capability: The TDC is designed to handle beam crossings which occur at a 7.5MHz rate (132ns crossing time). The BTeV DAQ requires that each detector report its data from every crossing into a data buffer. In order to handle this requirement, the TDC will need to sparsify its data, reporting only the channels which have been hit during the particular crossing. In order to achieve this, and to relax the instantaneous bandwidth requirements for the data output link, we plan to include a local FIFO which will average over statistical fluctuations in the data rate. The size of this FIFO is related to the excess bandwidth that our output links will have, and at this time is still under study. Under normal circumstances, the FIFO size will be large enough so that there will be a negligible probability that it will overflow on a 2∼3 hr time scale. However occasionally we expect abnormal conditions to arise (e.g. particle spray due a beam instability, or electronics oscillating). This could cause the FIFO to overflow. In order to handle these cases, we plan to flag and truncate new events when the FIFO reaches 80% of its capacity. When the FIFO depth lowers itself to the 50% occupancy level, new events will again be let into the FIFO input. In this way we should receive a selection of the offending events in order to plan an online fix to the problem (if its origin is due to the detector). Obviously there must be a monitor process running at the upper levels of the online software which is looking for these error occurrences. As mentioned above, our design was for a 132ns crossing time. However it now may be more likely that the crossings will be kept at the 396 ns level (36x36), but with an increase of events per crossing. As far as the electronics are concerned, 396 ns crossing is less difficult than the 132 ns case (a case of fratricide in our single hit TDC as occupancy rates increase), so we anticipate no difficulties with the TDC readout.

8.7.8 I/O Interface

8.7.8.1 I/O Introduction

The I/O interface is based upon a 7.5 MHz clock (132 ns), which is referenced to the Tevatron 53 MHz RF clock. The Tevatron RF structure has 1113 53 MHz rf buckets, which fill the circumference of the ring. The number 1113 can be factorized into 3, 7, and 53, which represent the RF symmetry of the Tevatron. The 7.5 MHz clock is just the symmetry given by 7 bunch spacing. There are 159 (3*53) of these ticks around the Tevatron. Beam can in principle be placed in any of the 1113 rf buckets, but typically is placed into the buckets given by the symmetry of the Tevatron and its injector (FNAL Main Injector). Typically 3-fold symmetry is used in the bunch loading scheme, so that the original BTeV running condition includes 3 trains of 36 bunches. Within a given train, the bunches are separated by 132ns. Since the future running may contain a different number of bunches: 3 x12—the current 396

ns spacing, or possibly 3 x 24 (264 ns spacing), it was decided to keep the original 7.5MHz clock requirement, because it could handle any of these beam scenarios. Gaps between trains (i.e. the incomplete filling of every possible "tick") is driven by the need to account for the rise and fall time of the Tevatron Injection Kicker Pulsed Magnets. The control of the TDCC is done on the reception of a command every 132ns. These commands may run from "Start TDC (and readout when finished)", to "Load ASDQ DAC Threshold buffer with new value", to "Read ASDQ DAC threshold buffer value", to simply "No Operation". In addition to the command itself, the reception allows the ASIC to resynchronize itself to the clock. This clock is used internally (at multiplied frequencies) for the TDC clock (1.56 ns is derived from the 12^{th} harmonic of the accelerator RF clock) and the Data output clock. If possible it will be used as the crossing timing clock, with the idea again to minimize the number of cables in the electronics. The command structure is still in its conceptual stages, but it will allow us to use (in principle at least) everyone of the 159 "ticks" as an operation. Operations which require data readout (such as "real" data, TDC calibration data and internal register readback) will, of course, be controlled from the application environment to be consistent with the output bandwidth of the datalinks and the BTeV DAQ. Separation of the data into the proper streams will be done in the Data Combiner Board (DCB). The following is a brief (and tentative) version of the expected commands.

- NOP: No operation this tick. Primarily use to keep clock synchronization
- Start TDC: The TDCs are strobed with a start pulse. When timeout occurs, data are placed in the TDC FIFO buffer and readout occurs as soon as possible.
- Start TDC Calibration: The ASDQ's are strobed with a calibration pulse whose amplitude and relative timing are given by respective registers. The TDC is also started. When timeout occurs, the data are placed on the TDC FIFO buffer and readout occurs as soon as possible.
- Load ASDQ Threshold Buffer: A new value is loaded into the ASDQ threshold register, which then strobes a DAC to supply the ASDQ with an analog threshold voltage.
- Load TDC Offset Value: A new value is loaded into the TDC Offset register. This time represents the relative offset to the actual bunch crossing from the decoded "Start TDC" timing. Used with the TDC Timeout Value to put a window around the valid TDC Data region.
- Load TDC Timeout Value: A new value is loaded into the TDC Timeout register. The time at which the TDC stops. Any TDC channel which has not registered a hit by this time is considered "empty" when the data is sparsified.
- Load Calibration Pulse Amplitude: A new value is loaded into the Calibration Pulse Amplitude register. This amplitude will be used to keep track of the ASDQ channel response.

- Load Calibration Pulse Delay: A new value is loaded into the Calibration Pulse Delay register. This will be used to track the TDC time calibration (although it isn't completely independent of the TDC timing).

In addition to all the load commands, there will also be a corresponding "Read" command, which will place the current value of the particular register into the TDC FIFO, with the "tick" tagging given by the reception "tick" of the "Read" command. Readout of the TDC FIFO will be asynchronous and "on demand" simply by there being data in the FIFO.

It appears at this time that the data output bandwidth can be successfully handled by two 636 MHz serial links (636 MHz=12*53MHz) per module. The clock will be recovered by standard techniques at the Data Combiner Board (DCB) receiver. There will be a readout every 132ns, whether there is data or not, simply to keep the clock synchronized. The sync readouts will be as minimal a length as possible, consistent with their function. As has been described, both crossing TDC data and readback register values and calibration data are in a single data stream. The separation of the streams will be done in the DCB, where the data "ticks" are known. "Real" data will be routed to the correct buffers by the DCB. It will be the responsibility of calibration/monitor software routines to give the DCB the correct routing for these data.

8.7.8.2 Overview of I/O Implementation

We present here a design for a system of moving data from the front-end electronics to the Data Combiner Board (DCB) and a mechanism for sending timing and control data to the Front End Module (FEM).

The design of the baseline system has been shaped by the following considerations:

- Radiation environment. Since radiation exposure for these electronics is anticipated to be on the order of 20 kilorad per year, all of the front-end electronics need to be designed to be radiation tolerant. For this reason, no commercial chips are used on the front-end.

  Although commercial rad-hard FPGAs are available, they have proven to be too expensive for our application. Fiber optic components are not used for the front-end electronics due to their susceptibility to radiation-induced scintillation.

- Electromagnetic compatibility. Crosstalk between signal lines can cause data errors either on the Data Combiner end (where event data is received) or near the front-end electronics (where control/timing data is received). It is critical that we avoid the introduction of noise in the detector system. For these reasons all front-end electronics need to be designed so as to avoid transmitting or receiving EM energy.

- Limited physical space. The physical design of the detector sub-systems is controlled by consideration of physics goals. Little room is available for front-end electronics and/or cables and connectors.

- Cable length. The location of the Data Combiner racks relative to the detector front-end electronics is not entirely settled. It is anticipated, however, that the cables for the front-end data transport will be between 10 and 20 meters in length.

- Limiting the cable infrastructure. There are several reasons for reducing the cable infrastructure as much as is practical. As mentioned above, physical space for cables is at a premium. Also, the mass of the cables is going to affect the design of the mechanical supporting structures for the detector. Another reason for limiting the size of the cable infrastructure has to do with the way that the BTEV detector is assembled within the collision hall. Most of the detector subsystems have to be installed sequentially. Limiting the number and volume of the cables will improve the efficiency with which we are able to assemble the detector in the collision hall during the available time windows, and to access the detectors for repair.

The trend in industry has been to utilize high-speed point-to-point serial lines, differentially driven, to efficiently move data. More recently, cable equalization chips have become commercially available which compensate for the frequency dependent characteristics of twisted pair (copper) cables.

The use of cable equalization has made it possible to move data faster and over longer distances using copper wire than was previously the case. An example is a system shown in one application note demonstrating the recovery of 3.2 Gbps serial data at the end of 100 ft, 75Ω, coax cable; with only 0.16 unit interval of deterministic jitter.

The baseline design takes advantage of these trends by using four point-to-point serial links, each implemented with a differentially driven twisted pair, to service each Front End Module.

The first differential pair (the "T/C link") sends beam crossing time and control data from the Data Combiner board to the Front End Module. Two differential pairs send event data in the other direction, from the FEM to the DCB. The last differential pair sends a 132ns clock (called the "Refclk") from the DCB to the FEM.

The following observations apply to the Event Data links, T/C link and Refclk links:

- Shielded, twisted pair, category 6 cable (or equivalent), with foil shields for each individual pair and an electrically isolated overall shield for the cable, are used to limit EM emissions and receptivity.

- Each differential pair is terminated at the receiver end with the characteristic impedance of the cable.

- Receiver-end cable equalization and transmitter-end pre-compensation are used for the event data channel and timing/control channel, respectively.

- CML ("current mode logic") is used for signaling in both directions.

- All data is encoded in the 8B10B format.

- A Running Disparity Counter maintains DC balance (where the same number of 0's and 1's are sent on each twisted pair) by selecting the disparity of each data word transmitted.

8.7.8.3 Reference Clock

The Reference clock (or "Refclk") is the only high precision timing signal provided to the FEM by the DCB. This clock is derived from the Accelerator RF system, has a period of 132ns and performs three functions. The first is to provide the FEM with a precise reference for the beam- crossing clock. The rising edge of the Refclk, as received at the FEM, occurs at the beam crossing time. Not every 132 nsec interval will have beam. Intervals with beam will have a bit set in the T/C data word, see section 8.7.8.4 below.

The second function of the Refclk is to allow the DCB and the FEM to each generate a local T/C link bit clock. The DCB uses a PLL to generate a local T/C link bit clock (20x the frequency of the Refclk) and uses this clock to send T/C link data in synchronization with the Refclk. Separately, the FEM uses a Delay Locked Loop to multiply the Refclk by 20 to generate its own T/C link bit.

The third function of the Refclk is to allow the FEM to drive the Event data link. The FEM uses the Refclk to generate the Event Data state clock (84 times the frequency of the Refclk). The Event Data state machine uses this clock to transfer data from the output buffer to the output shift register and for shifting the data out one bit at a time.

REFCLK and REFCLK* are sourced by the DCB and differentially driven using CML signaling. A CML- compatible commercial pre-emphasis chip is used to compensate for the frequency dependent characteristic of the cable.

8.7.8.4 Timing and Control (T/C) Interface

The T/C link sends beam crossing time and control data from the DCB to the FEM. A 20-bit T/C data word is sent every 132ns and the data is encoded in 8B10B format. The FEM takes the 132ns Refclk and uses a Delay Locked Loop to multiply it by 20 for use as a local T/C link bit clock to recapture the T/C link data.

Each T/C data word (16 bits after 8B10B decoding) is used to attribute certain markers to beam crossing intervals, and to implement a simple protocol for writing to and reading from the CSR registers within the FEM.

TCDAT and TCDAT* are sourced by the DCB and differentially driven using CML signaling. A CML- compatible commercial pre-emphasis chip is used to compensate for the frequency dependent characteristic of the cable.

T/C Data Format

Each Timing/Control word is transmitted in the form of 20 bits. The FEM uses an 8B10B decoder to detect the (10-bit) word boundaries and translates the 10-bit data back to 8-bit data using a lookup table. After 8B10B decoding, each Timing/Control word consists of 16 bits (2 contiguous 8-bit bytes).

The format for each word is shown below. Because the 16-bit T/C data is received as 2 contiguous bytes, the "high word" bit is used to mark which one is the MSB byte and which is the LSB byte. Data is always sent in big-endian format, where the MSB (with the 'High Word' bit set) comes before the LSB (where the 'High Word' bit is cleared).

MSB byte:	
7	'High Word' <= '1'
6	'BC' marker
5	'A' marker
4	not used
3:1	Function code:
	'0XX' no operation
	'100' write address
	'101' read address
	'110' write data
	'111' read data
0	Address/Data Bit 7
LSB byte:	
7	'High Word' <= '0'
6:0	Address/Data Bits 6:0

The 'BC' marker indicates that a 132ns interval (a 'tick') is occupied and that a collision may occur during this crossing. The 'BC' marker is '0' for all ticks within the Abort gap; the 'BC' marker is also '0' for 2 of every 3 ticks (not including the Abort gaps), when the accelerator is operation in 396ns mode.

The FEM will initiate the acquisition of physics data during each crossing that is designated with the BC marker, unless this operation is disabled by writing to one of the CSR registers in this module. It is therefore equivalent to a 'START_TDC' operation, for example.

The 'A' marker designates that a 132ns interval is 'Bunch 0' and the Tick counter (which increments on every rising edge of Refclk) should be reset to 0.

T/C Data Timing

Because T/C data is sent as a serial stream, T/C data that is received by the FEM during the interval starting at T+0ns is not fully received (and captured) until time T+132ns. The FEM holds each T/C word for another 132ns (until T+264ns), so that the on-board logic has a generous setup time before the markers are acted upon, on the rising edge of Refclk.

T/C CSR Register Access

Besides marking which 132ns intervals are designated as occupied and which one is Bunch0, the Timing/Control word also has the ability to command the FEM to either read a single CSR register (the data is tagged by the Register ID and added to the Output FIFO), or to write a 8 bit value to a designated CSR register.

- Write Address: In order to write to the address register, the function code is set to '100' and the Register ID (0...255) is written to the Address/Data field.
- Read Address: In order to read back the value of the address register, the function code is set to '101'. The value of the Address/Data field is ignored.
- Write CSR: Writing to one of the 256 available CSR registers is done by setting the function code to '110' and putting the data (value = 0...255) in the Address/Data field. The Write operation always assumes that a Register ID has already been written to the Address register.
- Read CSR: Reading a CSR register is done by setting the function code to '111'. The Address/Data field is ignored.

8.7.8.5 Event Data Interface

All event register data is written to an Output FIFO. A finite state machine on the FEM monitors the state of the Output FIFO and transfers data to the Event Data link whenever the FIFO is non-empty. The FSM transfers data from the Output FIFO at 63.6 Mbyte/s

This data is then encoded into 8B10B format using a lookup table, loaded into a shift register and clocked out at 12 x 53Mbps => 636 Mbps, and differentially driven on the (EVDAT, EVDAT*) signal pair.

EVDAT and EVDAT* are sourced by the FEM and differentially driven using CML signaling. A CML- compatible commercial cable-equalizer chip on the DCB (on the receiver end of EVDAT/EVDAT*) is used to compensate for the frequency dependent characteristic of the cable.

Event Data Format

The Event Data link is used to transfer the following from the FEM to the DCB:

- Physics data. Data resulting from the conversion from a physics detector system.
- Calibration data. Data resulting from artificial stimulation of the detector elements or front end electronics.
- Register data. Data resulting from a Read Address or Read CSR operation.
- Test pattern data. Data resulting from a special test pattern mode, for testing the operation of the T/C link or Event Data link.

The format of the data written to the Output FIFO will depend upon the specific system, however it must be structured in a way that allows the DCB to distinguish between these different data types and to associate data from the same event into some type of record. In most cases it will be necessary for the structure of the data to accommodate a variable record length.

8.7.8.6 8B/10B Encoding and the Disparity Counter

8B10B is the name of a data coding system where 8-bit data is translated via a lookup table into 10-bit code. This translated data has the property that the maximum run length of identical bits is 5, aiding in the recovery of the bit clock on the receiving end.

A second property of this coding system is the existence of a unique 'Sync' pattern that can be used to resynchronize the framing clock of the receiver with the transmitter. The Event Data state machine inserts 'Sync' words into the data stream whenever the Output FIFO is empty.

Each valid 8B10B character has a disparity of 0, +2 or -2. For every non-zero code, there exists an alternative code with the opposite disparity.

In order to maintain DC balance, the Event Data interface (on the FEM) and the T/C interface (on the DC) use a running disparity counter (RDC) to determine whether to use the positive disparity or negative disparity code for each data word.

8.7.8.7 Cabling

Cable Packaging Requirements

The proposed mapping of differential pairs to cables is based upon the following considerations:

- Some detector sub-systems (specifically the Straw detector) require 2 Event Data links per electronic package to accommodate the anticipated rate of event data, plus a nominal safety factor.
- The Refclk and T/C links are intended to support multiple receivers, so long as the following are true:
  - These signals are routed in daisy-chain fashion, where they visit one receiver then the second, where the transmission line is terminated.
  - The path length between the two receivers is no more than 1 cm.
  - The two receivers can distinguish between the registers on each by using different register addresses (where appropriate).
  - Standard rules for routing high speed differential signals are followed, including the following:
    - Use of a ground plane
    - Keeping the signals in differential pair the same length.
    - Stub avoidance
    - Via minimization
    - These signals should always maintain the same reference plane (the power or ground plane closest to the signal).

- Mixing near-end (transmitter) signals and far-end (receiver) signals on the same connector may cause crosstalk between the two, due to the fact that the near-end signal is going to be strong in amplitude and the far-end signal is going to be attenuated by the length of the cable.

Cable Packaging Design

The proposed cable definition uses two 2-pair cables, with 4-contact IEEE 1394 type connectors on each end:

Cable 1:	
Pin 1	Event Data(0)
Pin 2	Event Data_(0)
Pin 3	Event Data(1)
Pin 4	Event Data_(1)
Cable 2:	
Pin 1	RefClk
Pin 2	RefClk_
Pin 3	TCDat
Pin 4	TCDat_

Still under consideration is an alternative cable packaging plan consisting of the use of 4-pair, ISO category-6 shielded cables and category-6 RJ-45 connectors.

8.7.8.8 Customized Interface Circuit (ASIC)

Commercially available chips are used wherever possible within this design. On the other hand, an application specific custom IC is necessary to act as an interface on the FEM end. It is hoped that the uncommitted detector subsystems will be able to use the TDC ASIC planned for the straw detector system, taking advantage of the low incremental cost of producing additional chips.

8.7.9 Data Combiner Board (DCB) - Straw Daughter Card

As described above, the TDC ASIC has a built in command functionality, but no pre-knowledge of the beam time structure. That knowledge is based in a lookup table in a daughter card of the DCB, which has been specialized to the needs of the Straw Front end. This daughter card has a 159 element lookup table, one for each 132ns "tick". Each element has been loaded with one of the possible commands. This daughter card also contains the circuitry to run our input and output serial links.

8.7.10 Straw High Voltage System

The straw tube anodes will be biased by dedicated high voltage (HV) power supplies controlled and monitored by conventional slow control techniques. Each HV power supply channel will bias a set of 96 straw channels by applying voltage to the anode wires at both ends of a set of 48 straws. Thus a minimum of 558 HV power supply channels will be required. Each HV channel will be capable of applying bias voltages up to +2200 V, to easily accommodate the option of using 8 mm diameter straws in low occupancy regions of the tracker, and be able to source up to 200 μA of current, consistent with our Monte Carlo estimates of maximum occupancy levels and incorporating a substantial safety factor.

The HV power supply modules will be placed in relay racks and located in a low radiation area of the C0 interaction hall. Connection to the forward tracker will be through intervening multi-conductor cables and patch panels. HV will be distributed within a straw frame to individual straw channels via a high voltage bus built from double-sided printed circuit boards. Connection is made between the bus traces and HV voltage cards that connect directly to the straw anodes. Electrical tests have verified that the trace topology on the bus resists arcing well beyond any anticipated working high voltage. The final vendor for the HV system is not yet decided. Monitoring and control software will be developed after the final vendor is selected.

8.7.11 Straw Low Voltage System

The straw tube front end electronics will be powered by dedicated low voltage (LV) power supplies controlled and monitored by conventional slow control techniques. The LV supplies will power both the front end amplifier/discriminator card and the TDC card, and will need to provide ± 3 V. The precise current required is not yet known since the TDC cards are not yet designed. Similar to the HV power system, the LV power supply modules will be placed in relay racks and located in a low radiation area of the C0 interaction hall. Connection to the forward tracker will be through intervening multi-conductor cables and patch panels.

LV will be distributed within a straw frame to front end electronics cards via a bus built from printed circuit boards (PCBs). Prototype bus design has begun. Connection will be made between the bus traces and either the TDC card or the amplifier/discriminator card, whichever is more practicable. (Power would then be delivered to the other card via connectors joining the two.) The final vendor for the LV system is not yet decided. Monitoring and control software will be developed after the final vendor is selected.

8.8 Installation, Integration and Testing Plans

8.8.1 Summary of Testing Prior to Moving to C0

The Straw Detector will be assembled in half-views, including front-end boards and signal cables, and fully tested before moving to C0. Each wire will be tension tested and checked to see that it holds high voltage as it is strung, and then again when the half-view assembly is complete. Cabling and gas and cooling water lines will be attached and leak tested. The wire positions will be surveyed with respect to external fiducials on the half-view frames. Each half-view has an environmental sensor to monitor temperature and humidity; the readout from this will be tested. The functionality of the front-end electronics will be tested with pulses injected at the pre-amplifier inputs. The threshold voltages and other programmable registers will be set and read back. The full data readout chain will be tested with a radioactive source and/or cosmic rays.

8.8.2 Transportation of Straw Detector Equipment to C0

All straw detector equipment will be staged at Fermilab Lab 3 prior to moving to C0. Detectors will be moved as full stations for stations 1-6 and as super-modules for station 7. Equipment will be moved from Lab 3 to C0 by Fermilab Material Distribution Department trucks and drivers. The stations will be packaged for transportation on the tooling used for installation at C0. For transportation, frames will have casters attached to facilitate movement. Super-modules will be crated in either wooden boxes or on 'Unistrut' type frames. The straw half-views will be transported in half-view transportation frames. The transportation frames will have outriggers for stabilization and will accommodate casters for local movement.

Relay racks will be transported with standard tie-down precautions. The half-views may also be connected to a dry gas purge source during transportation. A transportation procedure will be prepared for the transportation operation.

All relay racks can be loaded and transported in one-half day. The smaller straw stations (can be loaded and transported in less than one-half day. The larger straw stations may require one or two full days for loading and transportation.

8.8.3 Installation of Straw Detector at C0

At C0 stations 1-6 will then be split into 2 half-stations – each with an X,U and V half-view attached to a back plate (see Fig. 8.26).

The half-station assemblies will be transported into the collision hall and moved into position with a dedicated cart. The cart will have provisions for safely positioning the assembly onto a rail system for docking. Stations 1-6 will first be mounted aound the beam-pipe at the mouth of the SM3 magnet. Before sliding them along the beam-line into their docking positions, utility connections will be attached and tested.

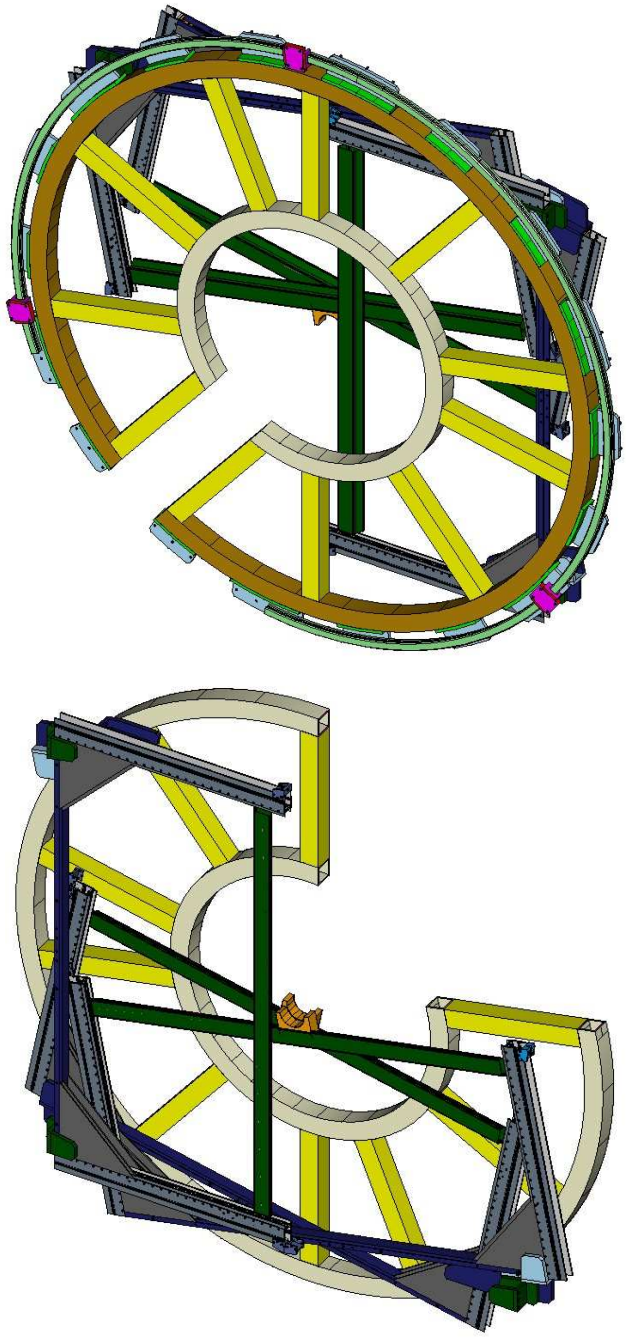

Figure 8.26: Straw Station assembly – 2 half-stations with back plates

Power supply cables and signal cables will be attached, then the fully assembled station will be slid into the proper z position with a set of longitudinal rails. Once at the proper z position the station will be lowered a few centimeters and attached to more stable support brackets. At this point the X-module for the silicon support can be slid into position in the gap in the X-view.

The straw stations must be installed in the following order: 1,2,3,6,5,4. Station 7 will be treated separately as it is in a very confined space between the RICH and the ECAL. The positions of the straw stations will be surveyed using external fiducials on the half-view frames.

8.8.4 Testing at C0

After installation the following tests will be done:

- Leak test gas and cooling water systems.
- Test temperature and humidity monitoring and check that power supplies are shut off in the event of a cooling failure, or if humidity is too high.
- Test gas monitoring systems (gas gain, drift velocity, contaminant level),check functionality and integrate into slow control system and database.
- Check that all modules hold HV.
- Threshold voltages and other programmable registers will be set and read back
- Test Front-end electronics with pulses injected at pre-amp inputs
- Test readout into Data Combiner boards

8.9 R&D , Open Design Issues

8.9.1 Prototype Detector

We have constructed a 2 module prototype detector for test beam studies and to explore construction issues (see Fig 8.27). The construction of a module proceeds as follows: the straws are cuts to the correct length and twisters are glued in; the three layers of straws are set up on a corrugated base to form a close-packed array; the end-plugs are inserted into the module end-plates and silver epoxy is injected into the region around the end-plugs; the endplates are attached to the straws; finally the outside of the endplates is potted with structural epoxy.

We have adapted the wire stringing fixture from the one used by Atlas. The 25 μm gold-plated tungsten anode wires are inserted into the straws by blowing a lead through, tying the anode wire to the lead wire and pulling the lead wire back. A weight is hung from the wire to

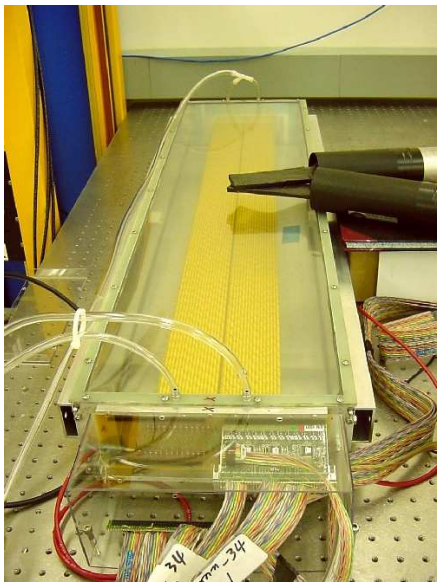

Figure 8.27: Straw prototype chamber

apply the correct tension. During production it will be necessary to have an efficient method of checking the tension of each wire as it is strung. We have set up an acoustic excitation method for measuring the tension – a loudspeaker is used to induce a mechanical resonance in the wire. A potential of 80V is put on the wire so the capacitance variation induces a signal. We use a LabView data acquisition system that generated a variable frequency to drive the loudspeaker and plots the response as a function of frequency. The resonance is easily observed.

The prototype is read out using COT cards (from the CDF Central Outer Tracker). Each COT card has three 8-channel ASDQ chips. The output of the COT cards is converted from LVDS to ECL via a translator board so we can use existing LeCroy TDCs.

We have done efficiency tests with cosmic rays and get a 95% efficiency for both Argon/CO2 and Argon/Ethane. This is as expected given the thickness of the kapton walls and some gaps due to out-of-roundness of the straws.

8.9.2 Straw Material

The first order of straws made with Kapton XC as described in section 8.4.2.1 above, were manufactured by Stone Industrial, Maryland. We found two major problems with these straws. They are not perfectly round making close packing difficult, and about 20% of the straws leak due to lack of glue between the 2 layers. We have since obtained a shipment of straws from Lamina Dielectrics, England, and are currently doing extensive quality control checks.

We have discovered that kapton loses tension when exposed to various gases, in particular it is very sensitive to even low levels of ethanol[7].

One of the gases considered for use is a 50:50 mixture of Argon-ethane; however this requires a small fraction of alcohol to be added to prevent aging. We will need to use a gas mixture without ethanol or a different straw material – eg. copper coated kapton or copper coated mylar. Mylar has a lower coefficient of hygroscopic expansion and lower gas permeability for all gases where data exists so may be a preferable material. It is not as radiation hard as kapton but that should not be a problem with the radiation levels expected at the straw chambers.

The specifications from Dupont claim that the gas permeability of mylar is significantly reduced (up to factor of 100) by a metalization layer, this probably applies to kapton as well. We have recently received a shipment of copper coated mylar straws. Unfortunately they appear to have a large number of surface defects of unknown origin. This is under investigation. We plan to order some copper coated kapton straws in the near future. The CKM experiment has done a number of studies of this type of straw and has had no problems.

Another problem with the Kapton XC straws is that we see a signifcant amount of dark current after exposure to radiation when using an Argon/Ethane/ethanol gas mixture (see section 8.9.4).

8.9.3 Gas Studies

Since the use of an Argon-ethane gas mixture in the kapton straws is problematic (see section 8.9.2), and since additives such as CF_4 are not desirable because of their corrosive effect on the glass capillaries, we have studied various mixtures of Argon-CO_2 as a possible gas for the BTeV straw detectors. Another advantage of Argon-CO_2 is that it is not susceptible to the polymerization which occurs when hydrocarbon gases are used in a high rate environment. The various features that have been investigated include:

- gain
- efficiency
- operating voltage
- drift time
- spatial resolutions
- after pulse frequency
- streamer frequency

We have investigated these performance parameters with a range of Argon/CO_2 mixtures. We have compared the measurements with Garfield[8] simulations, and have also used Garfield calculations to determine expected behavior of the various mixtures for all parameters except the after pulses and streamers.

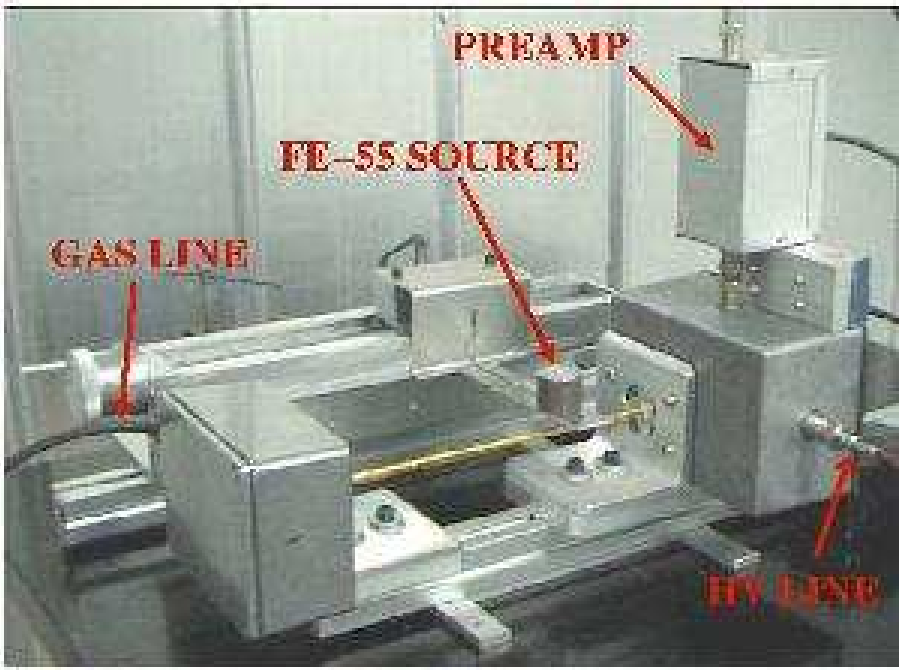

Figure 8.28: The short single straw prototype and ^{55}Fe source configuration for the Ar/CO_2 tests

8.9.3.1 Gain

An ^{55}Fe photon source (5.9 keV energy) was used to determine gain of the various gas mixtures. The ^{55}Fe photon interactions in the Argon produce an average of 210 e- in a very localized region (100-200 μm) so the intrinsic gain of a particular gas mixture at a given voltage can be determined by measurement of the integrated charge of the straw signals. The gas mixtures have been tested with the short single straw prototype arrangement shown in Fig 8.28. The straw is 4 mm in diameter with a length of 220 mm. The anode wire is 25.4 μm gold-plated tungsten.

Measurements of efficiency plateau, gas gain, drift time, pulse shape and other parameters have been performed to provide a baseline for other mixtures and to determine the reliability of the Garfield simulations. Once the Garfield simulation was verified, it was used to predict the efficiencies and spatial resolutions of the straw detector.

Initially, we purged the straw with Argon-CO_2 80/20 at a high rate (14 cc/min) and then studied the dark current as a function of voltage. We found that the straw drew 0.1-2 na current between 800 and 1500V (the voltage range determined to be appropriate for this mixture).

After purging, the straw detector was exposed to the ^{55}Fe source. The pulse shapes due to the ^{55}Fe photon interactions were investigated and compared to Garfield simulations. Shown in Fig 8.29 is the average of 250 pulses at 1300V from the straw before the preampli-

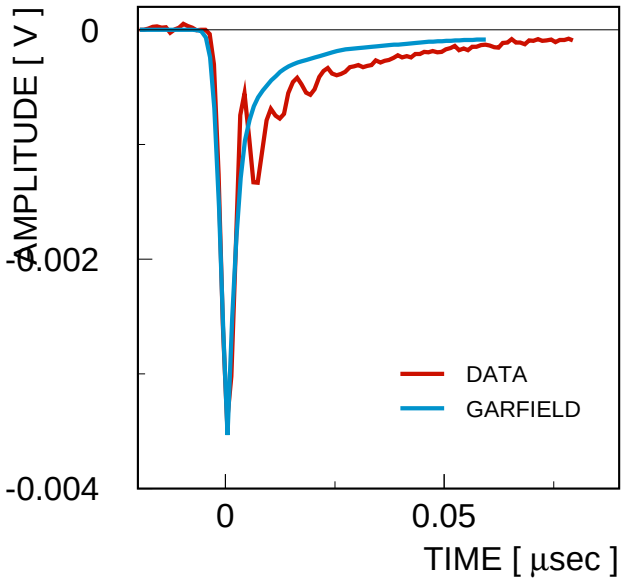

Figure 8.29: Comparison of pulse shapes from data and Garfield simulation

fier. For comparison, we show the average of 33 pulses simulated in Garfield. There is good agreement generally. The post-amplifier pulses were also compared with a Garfield simulation that included a simulation of the amplifier and were found to be in good agreement. From these studies we determined that integrating over a 300ns gate applied to the pulse obtained directly from the straw would capture 55% of the charge generated by the photon interactions.

The pulse height spectrum resulting from integrating over 300ns is shown in Fig 8.30 Both the K shell escape peak and the full peak are quite visible. The measured ratio of energies of the two peaks is 2.20, in good agreement with the expected 2.19. The measured escape fraction of interactions is 14.6% also in good agreement with the expected escape fraction of 15%.

To determine the intrinsic gain of the 80/20 gas mixture, a 300 ns integration of pulses directly from the straw using the integration function of a fast scope was performed, On average, after subtraction of pedestal and allowing for the 55% collection efficiency of a 300ns gate, the 5.9 keV ^{55}Fe photons produced an average charge of 4 pC at 1450V. Using 210 e- as the average charge deposited by the average of the escape and full peaks in this spectrum, the intrinsic gain was determined to be 1.2×10^5 at 1450V. Using this technique, the two points labeled as "scope" in the gain vs. voltage shown in Fig 8.31 were obtained. We also measured the integrated charge post preamplifier vs. gain to obtain the variation with voltage over a wider range of voltage. We have used a FOCUS/BNL831 amplifier whose gain has been measured. We also incorporated a simulation of the amplifier in the Garfield simulations. However, since the preamplifier pulse shaping loses a large and unknown fraction of the charge, the scope measurements were used for absolute normalization of the post

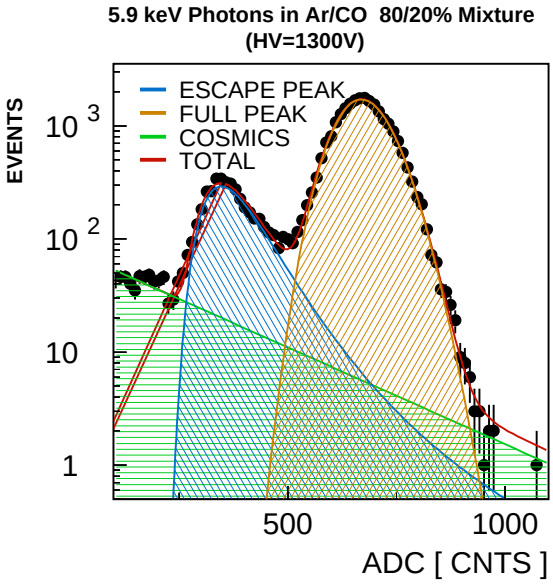

Figure 8.30: Pulse height distribution from Ar/CO_2 80/20 mixture from 5.9 KeV photons from a ^{55}Fe source. The dots are the measurements and the red line is the fit of two skewed Gaussian distributions on top of an exponential background due to cosmic rays.

preamplifier measurements. The Garfield simulation of the gain vs. voltage curve is in good agreement with the post preamplifier ADC measurements except at the highest voltages which show some sign of saturation. The lowest voltage achievable was determined by the noise level from the straw which is equivalent to 27 fC deposited at the wire. This noise prevented us from operating at much below 1100V for this particular mixture.

8.9.3.2 Operating Voltage

The plateau curve shown in Fig 8.32 was obtained for the Ar/CO_2 80/20 mixture using an ^{55}Fe source and setting the threshold of the discriminator just above the noise level. As can been seen, the plateau is more than ample for operation using 80/20 Ar/CO_2 as the gas for the straw detector.

8.9.3.3 Drift Velocity

The drift time for the Ar/CO_2 80/20 mixture was measured using collimated ^{106}Ru β source with a 3.5 MeV end point which illuminated the entire straw diameter. The TDC spectrum shown in Fig 8.33 was accumulated using a scintillator signal as start and the straw signal as a stop. Full width at 20% of height is 33ns and base to base is less than 50 ns, so an Ar/CO_2 80/20 is certainly more than adequate for a 396 ns bunch crossing frequency for 4 and 8 mm straws. It also seems just adequate for a 132ns crossing frequency for the two sizes of straws.

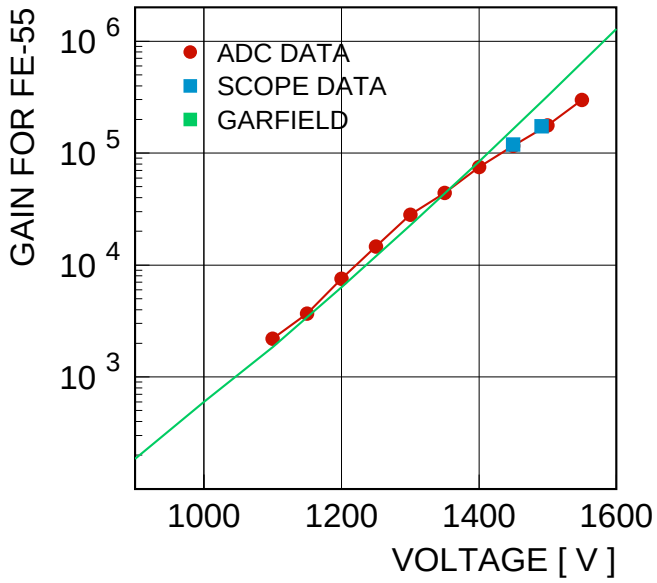

Figure 8.31: Gain vs. Voltage for Ar/CO_2 80/20 mixture. The solid line is the expected dependence of the gain on voltage from a Garfield simulation. The squares are actual measurements before the preamplifier, obtained using the integrating feature of the scope. The circles are post-amplifier measurements, obtained using an ADC, which have been absolutely normalized using the scope data.

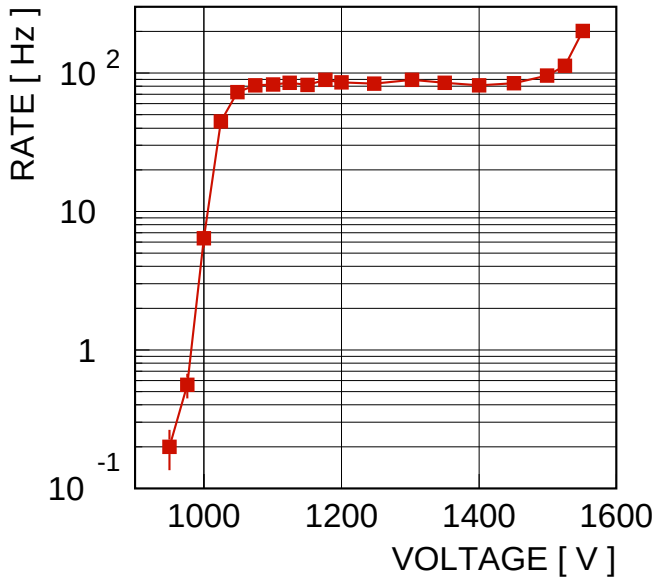

Figure 8.32: Plateau obtained for Ar/CO_2 80/20

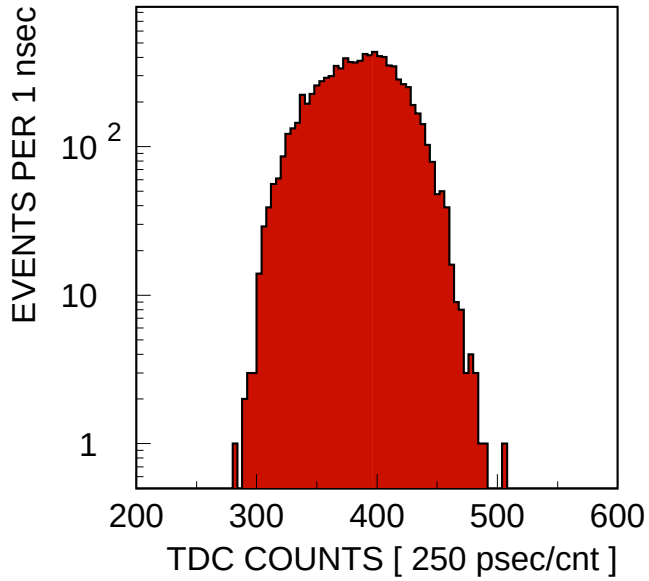

Figure 8.33: TDC distribution for 80/20 Ar/CO_2

8.9.3.4 Straw Efficiency

The efficiency for minimum ionizing particles passing through the straw at different distances from the anode wire can be predicted as a function of applied voltage using Garfield. The Garfield threshold is varied until the threshold behavior of the plateau curve of Fig 8.32 is matched by the Garfield simulation. To obtain a good fit to the data, the pulse shape post preamp had to be simulated well since the discriminator threshold is applied after the preamp. Once this was accomplished, curves of efficiency vs. distance of the minimum ionizing track from the anode wire (as shown in Fig 8.34) were obtained for the 80/20 mixture. As can be seen, to have acceptable efficiencies over the majority of the straw diameter, the straw must be operated at a voltage $>$ 1350 V.

8.9.3.5 Spatial Resolution

Using the Garfield simulations of efficiency we can also predict the intrinsic resolution of a gas mixture at a given voltage by studying the correlation of time versus distance. The simulations predict the range of distances from the anode wire corresponding to what is observed, i.e. the time of arrival of the electrons at the anode wire. A plot of resolutions obtained from a the fit of the distributions of distances corresponding to given times is shown in Fig 8.35 for several voltages. Once again, in order to obtain "intrinsic" resolutions (ones which do not include any uncertainties due to the experimental algorithms used to translate times to distances) better than 100 μm, the operating voltages for the 80/20 mixture must be set above 1350V.

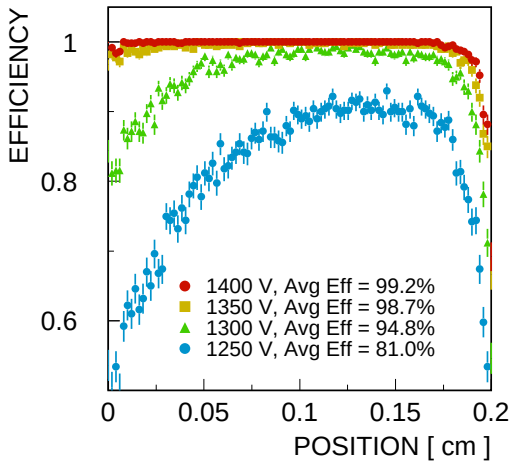

Figure 8.34: Garfield calculations of efficiencies for minimum ionizing particles vs. distance from the anode wires for an 80/20 Ar/CO_2 mixture at various voltages.

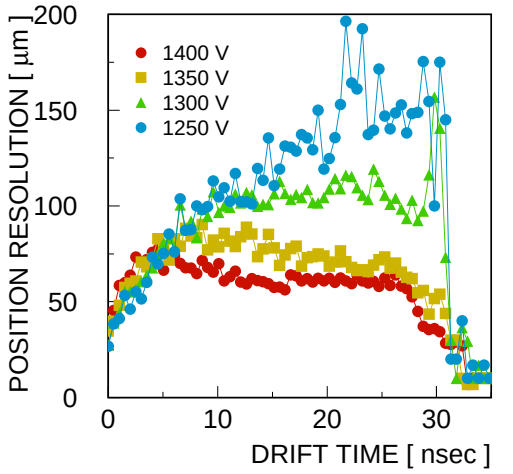

Figure 8.35: Garfield calculations of "intrinsic position resolution vs. drift distance at a variety of voltages

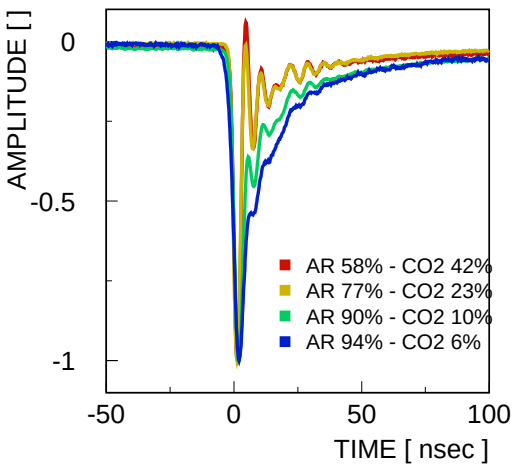

Figure 8.36: Variation of observed pulse shape with percentage CO_2

8.9.3.6 Streamers and After-pulsing

Without a quenching component, a gas such as Ar/CO_2 is more prone to large Geiger type pulses (streamers) or after-pulsing due to interaction of secondary photons in the walls of the straw. We have started studying the prevalence and voltage onset of these phenomena.

8.9.3.7 Other Ar/CO_2 Mixtures

Varying the percentage of CO_2 changes the performance of the straw dramatically in some case. In Fig 8.36, the behavior of the pulse shape is shown as observed for several gas mixtures. As the percentage of CO_2 is decreased, the pulse broadens in time, an undesirable effect. Fig 8.37 shows gain vs. voltage curves for the various Ar/CO_2 gas mixtures.

Taking the ratio of observed gain divided by the exponential fit of the gain vs. voltage variations for the various mixtures, we obtain the curves shown in Fig 8.38. We observe the onset of saturation effects around 2×10^4 gain for all Ar/CO_2 mixtures but is less pronounced in the mixtures with lower $C0_2$ percentages. In addition, the dramatic increase in pulse height that signals the beginning of the streamer mode occurs earlier and in the mixtures with higher CO_2 content.

In Fig 8.39 is shown the drift time distributions obtained using the ^{106}Ru beta source for a number of gas mixtures. As can be seen, the time distribution broadens with decreasing CO_2 percentage, also an undesirable effect.

The increase of drift time with decreasing CO_2 content is shown in Fig 8.40 compared to the expected changes of drift time with CO_2 percentage obtained from Garfield simulations. As can be seen, the agreement is excellent.

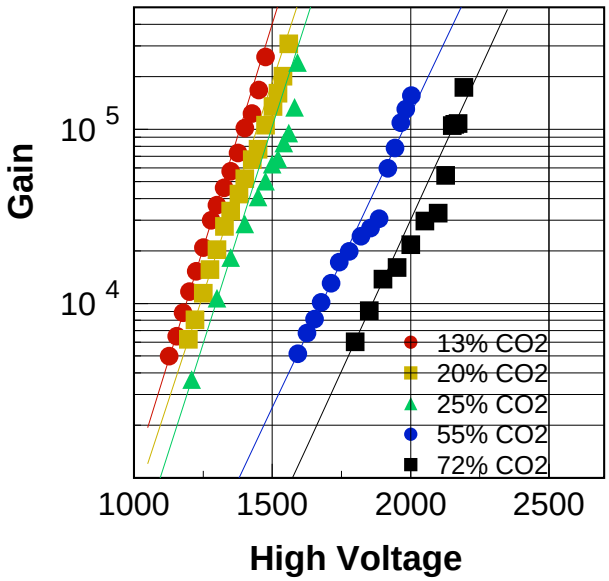

Figure 8.37: Gain as a function of HV for several Ar/CO_2 mixtures

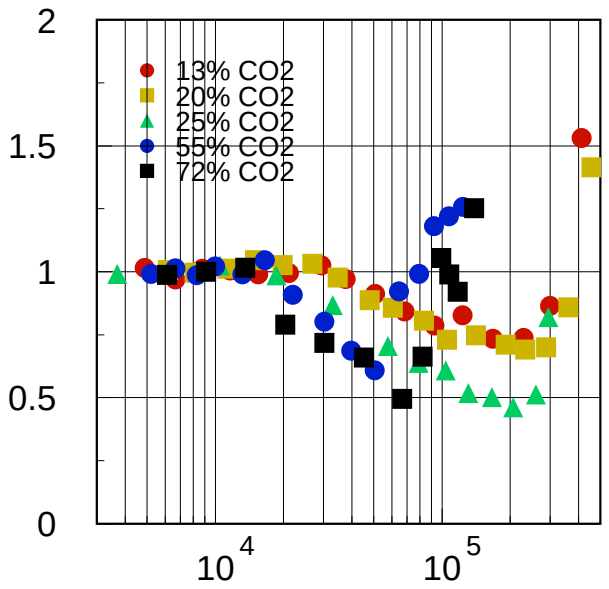

Figure 8.38: Ratio of measured gains to Garfield predictions for various Ar/CO_2 mixtures.

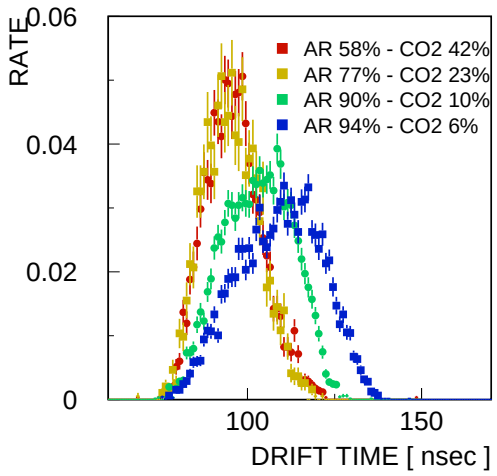

Figure 8.39: Time distribution for various Ar/CO_2 mixtures

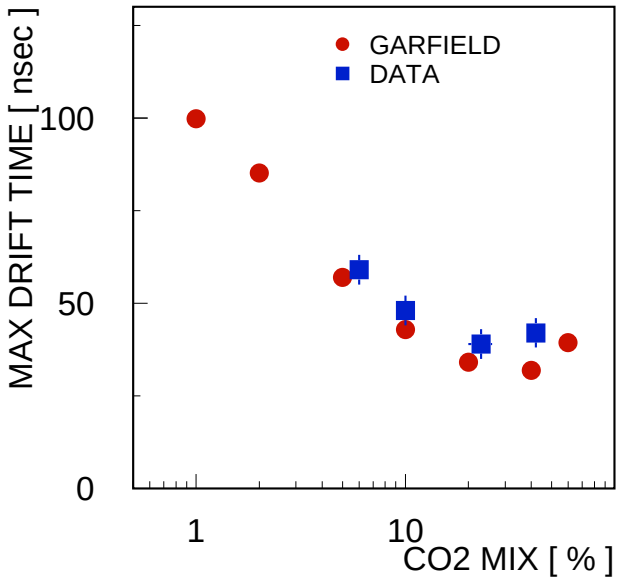

Figure 8.40: Variation of drift time with CO_2 percentage. The squares are measurements. The circles are Garfield calculations

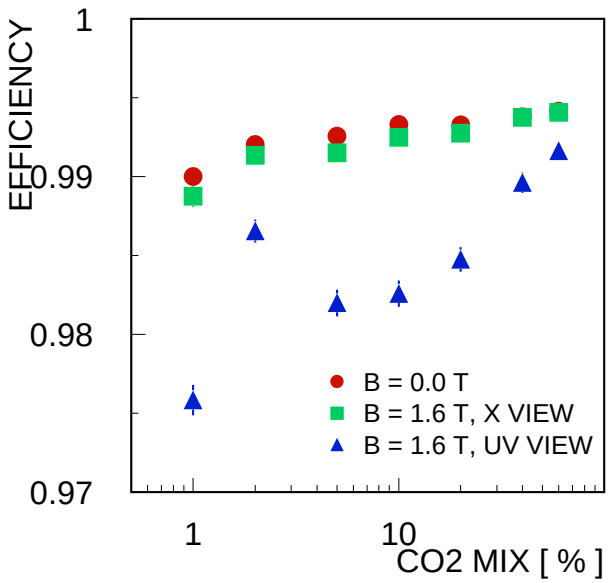

Figure 8.41: Garfield predictions of efficiency vs CO_2 percentage for no magnetic field and for 1.6T axial (UV) and transverse (X) fields

Finally, Garfield predictions of the variation of efficiency with percentage CO_2 is shown in Fig 8.41 at zero field (all calculations are made at an effective gain of 10^5 for the given gas mixture). Included are predictions for 1.6T axial and transverse fields. A small amount of efficiency is lost in the axial field configuration but the overall performance is still expected to be acceptable.

The general conclusions from the simulations is that the correct percentage of Ar/CO_2 should be greater than 10% for fast drift times but less than 30% to keep operating voltages as low as possible.

8.9.4 Aging studies

8.9.4.1 Introduction

We have done extensive aging studies for the straws for a number of candidate gas mixtures, including argon/ethane (50/50) and argon/ethane (50/50) with 0.5% ethanol, at different dose rates. We have done preliminary studies with argon/CO_2. The gain of the chamber is monitored by a Fe-55 source. The loss of gain is parameterized as the percentage gain loss per Coulomb of charge deposited on unit length of the wire. We analyze the wire and the cathode by Scanning Electron Microscopy (SEM) and Energy Dispersive Spectra (EDS) after each exposure to look for damage and deposits.

8.9.4.2 Description of the tests

We have constructed several short (40-60 cm) straw chambers for the aging tests. The straws are of standard design (Kapton XC). Each single straw is tensioned to 250 g between two gas boxes which are fixed on a rail. The anode is 25 μm diameter gold-plated tungsten wire, strung to 50 g tension. The gas mixture is prepared from argon (99.95% pure) and ethane (99.0% pure in liquid form) bottles by electronic mass flow-controllers. The ratio of argon to ethane was fixed to 50/50 to take advantage of a large body of experience with this gas mixture in the literature [9]. The gas flow-rate is typically 8-10 cc/min. Taking the volume of the gas boxes into account, this corresponds to about 10-50 volume changes per day. This gas flow-rate, while high compared to what is expected for the actual experiment, removes uncertainties about the aging results. The high voltage for the chamber is supplied by a stand-alone HV power supply whose current is monitored to detect the presence of dark current.

8.9.4.3 Gain measurements

The straw chambers were exposed to a radioactive source to accelerate the aging. The source is a 100 mCi ^{90}Sr β emitter which has a half-life of 28.5 y. The end-point energy of the electrons is 0.546 MeV. The electrons are collimated to about 0.5 cm in width. The width of the irradiated area of the straw is increased by the scattering of the low energy electrons in air. The width of the irradiated area of the straw is determined independently by a Geiger Counter and from the measured width of the gain profile. In most cases, we observed widths ranging from 0.5 to 1.0 cm. The peak dose on the wire is computed based on the total charge from the HV power supply assuming a Gaussian irradiation profile. The gain of the chamber in the irradiated region is measured by a Fe-55 source periodically. The 5.9 keV photons from Fe-55 source convert to about 230 ionization electrons in the chamber. The signal from the chamber is integrated by an oscilloscope or an ADC. The absolute gain is determined by integrating the Fe55 signal without amplification for 200-300 ns.

Table 8.4: Summary of aging results for argon/ethane (50/50) gas mixture

Dose rate (C/day)	Total dose (C)	Peak dose (C/cm)	Loss of gain (%/C/cm)	Other observations
0.01	0.1	0.05	< 5	No detectable loss of gain
0.02	1.2	0.5	50	No dark current
0.4	0.7	0.7	20	Total loss of gain after 2 days Gain recovered to 80% of initial value after 2 weeks

8.9.4.4 Results with argon/ethane

We have done several aging tests with the argon/ethane (50/50) mixture at different dose rates. The results are summarized in Table 8.4. We started with a low dose rate of about 0.01 C/cm/day up to about 0.1 C. The loss of gain was not noticeable. The test was repeated with a dose rate of 0.02 C/day for about 60 days. The loss of gain was significant when the dose reached 2 C/cm. The loss of gain is attributed to deposits on the anode wire, confirmed by SEM and EDS studies which showed extensive deposits on the wire (see Fig. 8.43. It is noteworthy that there was no visible damage to the cathode. We also did not observe dark currents in this gas. We have also investigated the case when the dose rate is very high, about 0.4 C/day. The chamber completely lost its gain after 2 days of irradiation. After purging the chamber with the same gas mixture for about 2 weeks, the chamber recovered 80% of the gain, having a permanent loss of about 20%.

8.9.4.5 Results with argon/ethane with 0.5% ethanol

It has been reported in the literature that additives such as water and ethanol can slow down the aging of wire chambers. We have therefore conducted an aging study with the argon/ethane (50/50) mixture laced with 0.5% ethanol. The ethanol (90% pure) was kept at -1 degree C by a chiller. The percentage of ethanol in the mixture, based on calculated saturated vapor pressure of ethanol at -1 degree C, is 1.5%. We diluted the gas by a factor of 3 to reduce the ethanol content to 0.5%. The choice of 0.5% was based on some prior experience with this gas mixture. The straw was aged in the same way as in the case without ethanol. A preliminary aging test was done for 10 days at a dose rate of about 0.1 C/day. The accumulated peak dose was about 0.5 C/cm. We did not observe any loss of gain at this dose. We then irradiated a different region of the same chamber for 20 days at the same dose rate. At the end of the aging process, the gain profile showed an average gain loss of about 8%/C/cm, significantly lower than the case without ethanol. We, however, observed appreciable dark currents after a dose of about 0.7 C. The current is source induced; the dark current dropped to zero when we removed the source, but the dark current was re-ignited when the source was reintroduced. The results are summarized in Table 8.5.

Table 8.5: Summary of aging results for argon/ethane (50/50) with 0.5% ethanol

Dose rate (C/day)	Total dose (C)	Peak dose (C/cm)	Loss of gain (%/C/cm)	Other observations
0.1	1.0	0.5	< 5	
0.1	4.3	1.7	8	Substantial dark current was observed after 0.7 C total dose

8.9.4.6 Results with argon/carbon dioxide (80/20)

As described in section 8.9.2, other concerns of the straw materials have prompted us to consider using an argon/CO_2 gas mixture for the straw chambers. Gas mixtures without hydrocarbons are known to be more resilient to aging under harsh radiation environment. On the other hand, it has been reported in the literature that anode aging in argon/CO_2 mix is very sensitive to silicon impurities[10]-[12]. We have constructed a somewhat longer (80 cm) prototype straw chamber to study the aging in an argon/CO_2 mixture. We started with an argon/CO_2 ratio of 80/20. The experimental setup and aging conditions are similar to previous tests. We have done three aging tests at different dose rates using separate regions of the same chamber. The first test was done at a rather high dose rate of about 0.1 C/day. We observed a significant loss of gain, of the order of 50%, after a dose of 2 C/cm. The second test was done at about the same dose rate and the loss of gain in the second test $\sim 40\%$ at 2 C/cm was consistent with the observation of the first test. We continued the second test to 4 C/cm, and observed 60% gain loss. The third test was done at a dose rate of 0.07 C/day. We did not observe significant loss of gain until the dose reached 0.6 C/cm, at which point the percentage loss of gain is about 8%. The results are summarized in Table 3. We will continue the third test until we reach a dose of 1 C/cm. We plan to do SEM and EDS scans of the three irradiated regions after the third test. In all the aging tests done with argon/CO_2, we did not observe any significant (< 50 nA) dark current. The results are summarized in Table 8.6.

Table 8.6: Summary of aging results for argon/CO2 (80/20) gas mixture

Dose rate (C/day)	Total dose (C)	Peak dose (C/cm)	Loss of gain (%/C/cm)	Other observations
0.1	2.0	2.0	47	No dark current observed
0.1	4.0	4.0	60	No dark current observed
0.07	0.6	0.6	8	Test in progress, no dark current observed

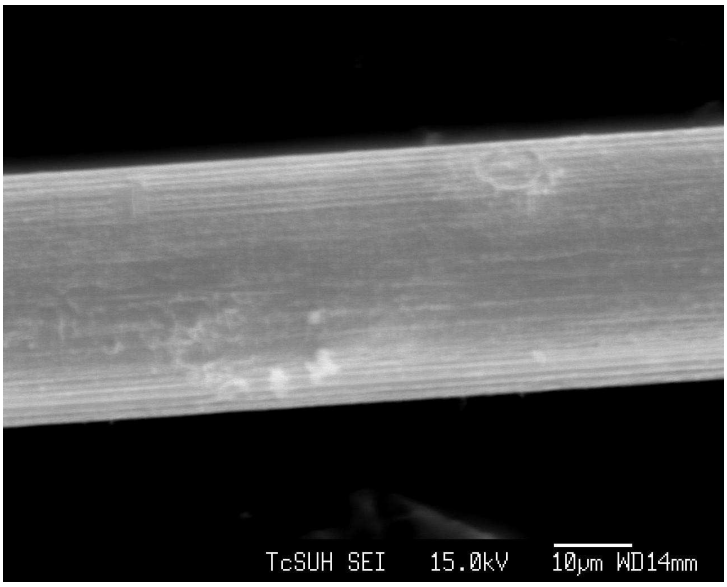

Figure 8.42: SEM picture of a wire far away from the irradiated region. Some imperfections of the wire (streaks and dimples) are visible.

8.9.4.7 SEM/EDS scans

We analyzed the aged wires by Scanning Electron Microscopy (SEM) and Energy Dispersive Spectra (EDS). In a typical run, a 15 keV electron beam impinges on the sample while the emitted X-rays from the sample are analyzed. The SEM image of a good wire is shown in Fig. 8.42 where the streaks of the drawn wire are visible. One can also see some other forms of imperfections on the wire, such as a "dimple" in Fig. 8.42. Fig. 8.43 shows a wire that was exposed to about 1 C/cm of radiation in argon/ethane; the deposits are very visible. The corresponding EDS spectrum provides an elemental analysis of the deposits. Most of the deposits have high carbon content, even though other elements were also seen.

8.9.4.8 Conclusions

We have studied the aging properties of straws in argon/ethane (50/50) mixture with and without ethanol and argon/CO_2 (80/20). Argon/ethane alone shows significant aging at the level of 1 C/cm, the expected total dose in 10 years of running in the worst region. The addition of 0.5% of ethanol to the mixture improves the aging performance of the chamber. The loss of gain is below 10% after a dose of 1 C/cm, but the chamber shows significant dark current after about 0.7 C. Argon/CO_2 looks very promising both in retaining gain and not showing dark current at the dose level of 1 C/cm. We will continue the study to optimize its aging performance.

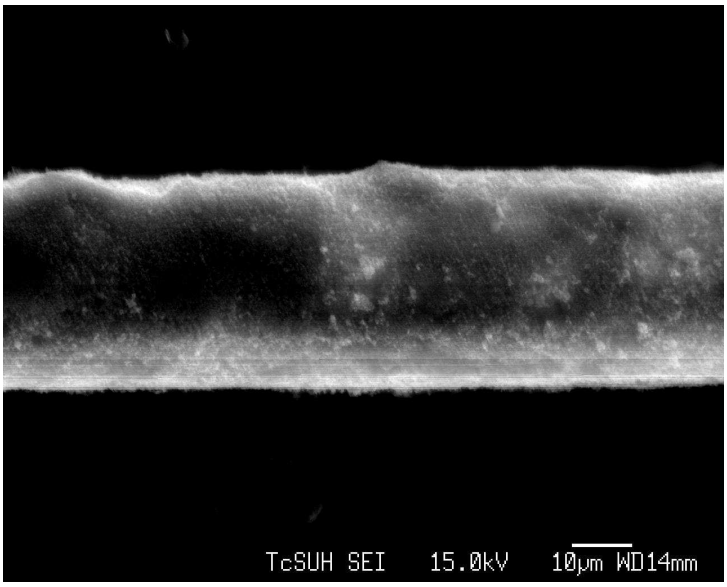

Figure 8.43: SEM picture of an aged wire. The dose of this region is about 1 C/cm.

8.9.5 Capillary Fusing

Because of hit occupancy of individual straws, the anode wires of each straw will be divided into two parts using a glass bead "capillary" as the joint between the two segments of the wire. The technique has been used in Atlas Transition Radiation Tracker.

The adoption of glass capillaries as the joints for the segments immediately restricts the use of certain minority components of the gas mixtures such as CF_4 which was found by Atlas to have a corrosive effect on the glass beads.

The process by which the capillary is inserted and fused to the two wire segments is schematically shown in Figure 8.44.

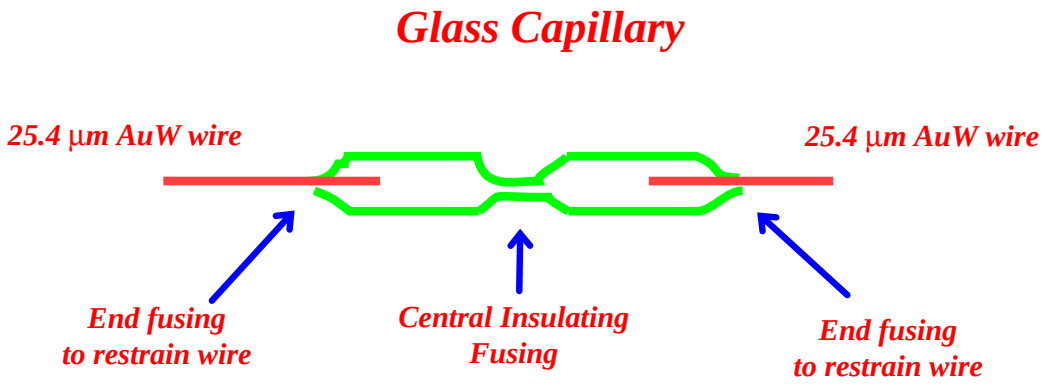

Figure 8.44: Capillary Fusing Technique

As shown in Figure 8.44 there are three fuse points required to join anode wire segments together within the straw. The central fusing is done to insure that the wire segments are electrically insulated from each other. The two end fuses are, obviously, done to provide the mechanical connection between the two segments of the wire.

Based on an estimate of approximately 26K anode wires, this procedure requires some 78K fusing operations. Thus, attention to ease and efficiency of the technique is important. The capillaries themselves are prepared by cutting a glass tube into 6 mm segments with a diamond saw to insure smooth ends. Once the capillaries are prepared and ready for fusing, the fusing operation is done in two steps using two different fusing devices. The central fusing is performed on one device and the resulting capillaries are inspected under a binocular microscope to insure that the capillary is closed. This operation will proceed in parallel to the second end fusing operation insuring a supply of centrally fused and inspected capillaries will always be available to for the second stage end fusing operation.

In the end fusing operation, the anode wire is spooled out to a predetermined length and cut. The ends of the 25 μm gold-plated tungsten wire are inserted by hand using a microscope for positioning into the ends of the centrally fused capillary. The ends are then fused to complete the process. The anode wire together with its capillary is then spooled up to be later unspooled when the wire threading into the various straws is performed. The results of both fusing processes will be recorded by digital camera and a record will be kept on disk for inspection by a supervisor at the end of each shift.

Shown in Fig 8.45 is an overall picture of the prototype fusing mechanism that has been developed at the University of Virginia to accomplish this task. The propane flame used to melt the glass is visible as well as the tongue and groove arrangement for placement of the capillary.

Fig 8.46 shows a view through a binocular microscope of the capillary as it is placed in the holding groove. The configuration of the groove and tongue/slot. is the configuration for central fusing. The extension of this prototype to the configuration for the end fusing is simply a double propane flame and two tongue/slot arrangements for either end of the capillary.

Fig 8.47 shows the capillary being transported through the propane flame by an automated system consisting of a motor/screw-jack arrangement. The height of the capillary above the flame, the temperature of the flame (1100^{o}C), and the speed of the transport through the flame were all carefully adjusted.

In addition, the capillary must be restrained since the velocity of the propane gas in the flame is enough to distort the capillaries. All of these parameters have been studied and determined with our prototype and capillaries have been successfully fused. Fig 8.48 shows a successfully center fused capillary.

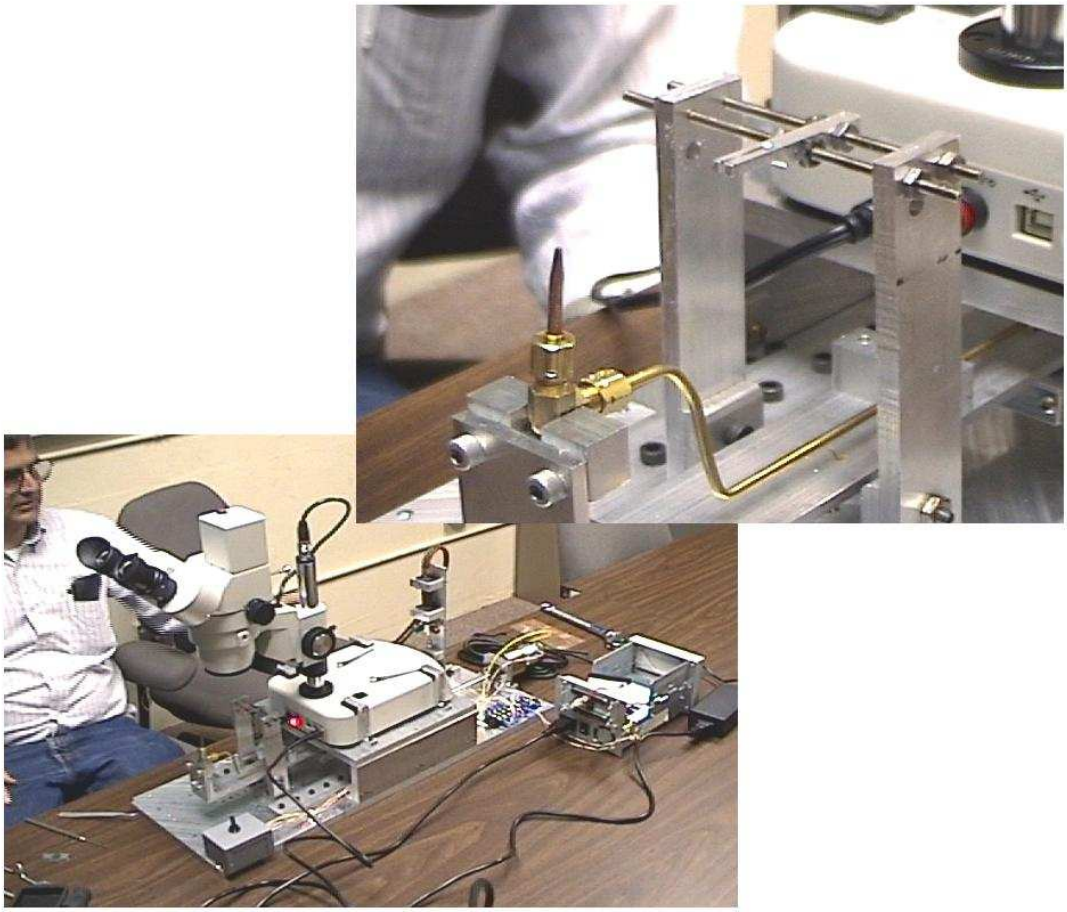

Figure 8.45: The UVa Prototype Capillary Fuser

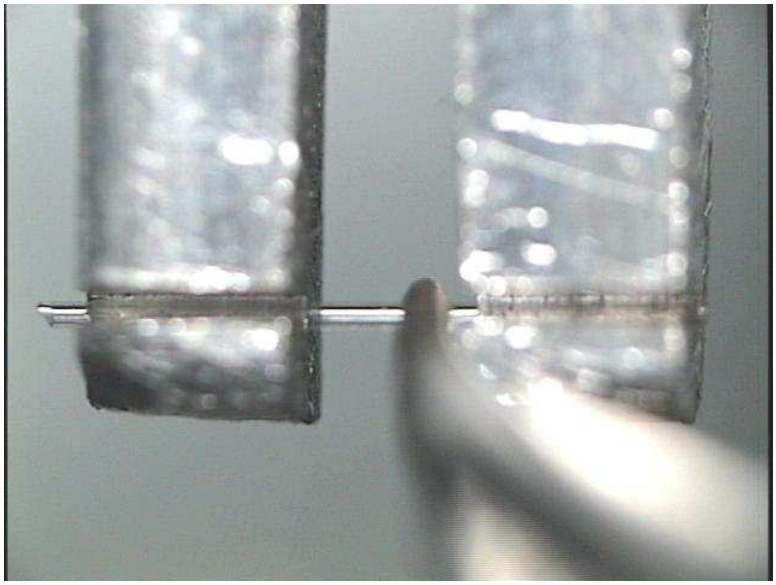

Figure 8.46: Tongue/Groove for seating capillary

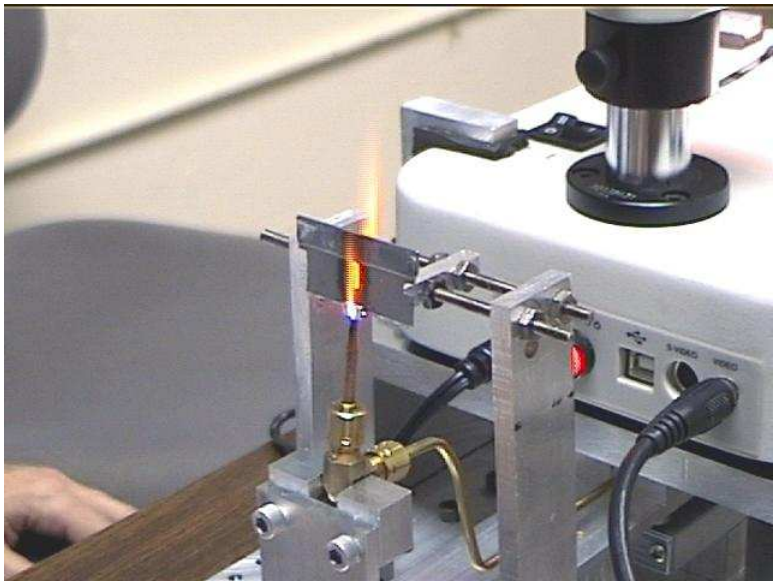

Figure 8.47: The restrained capillary is transported through the 1100^{o}C propane flame

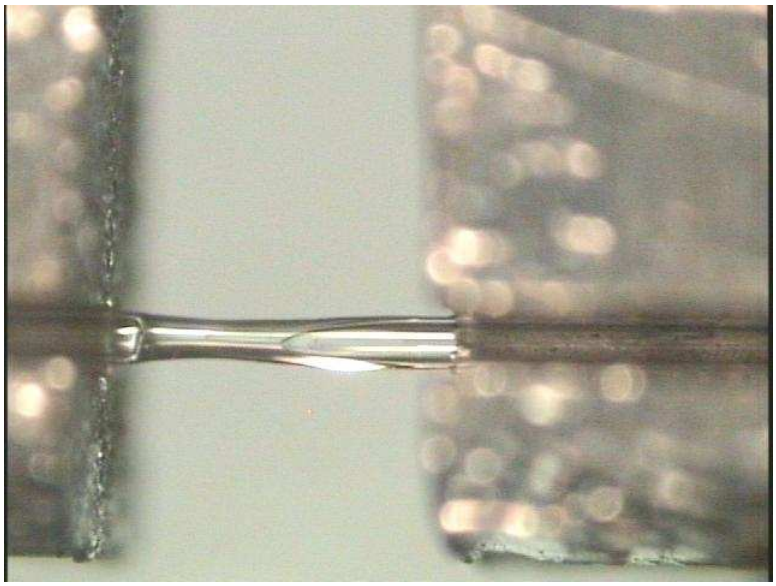

Figure 8.48: A centrally fused capillary

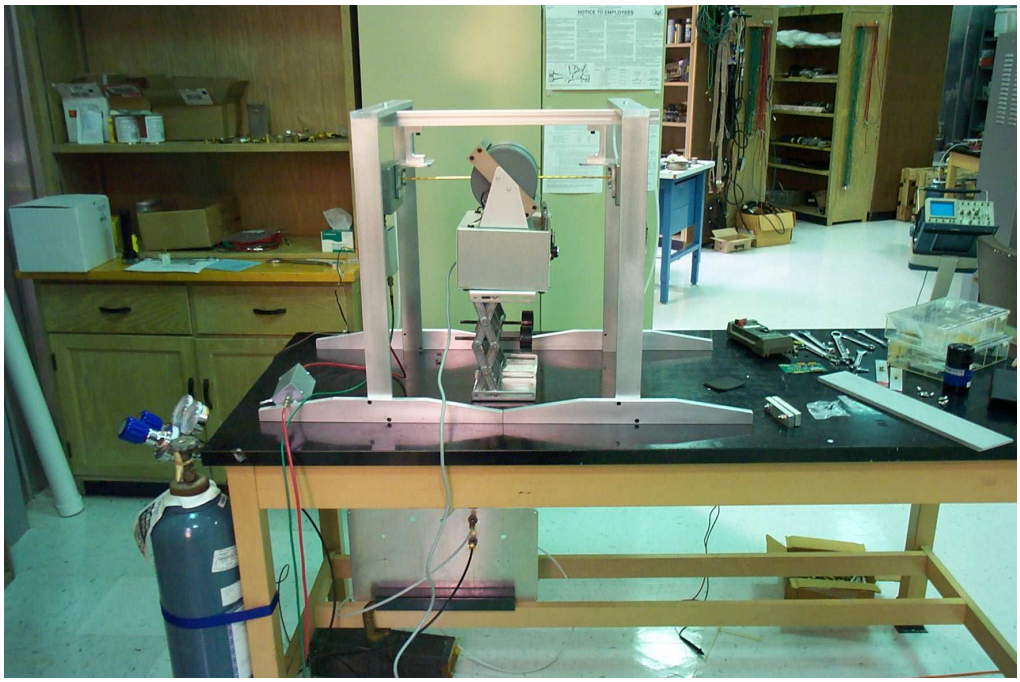

Figure 8.49: Electromagnet/Single Straw Prototype Test Setup

8.9.6 Magnetic Field Effects

Some of the straw chambers will operate within a magnetic field of 1.6T (oriented in the horizontal direction). Thus a 1.6T field will be imposed transversely on the vertical straw chamber views of Stations 1 and 2 (and with a lesser field on Station 3). The two 11^o views will have an almost axial field imposed on them.

Therefore, studies of the effects of the transverse and axial fields have been started to see if there is any loss of amplitude or distortion of the time distributions due to these fields.

While a full 1.6T field could not be obtained, we have done studies of transverse field effects studies using an electromagnet that produced a 0.75T field transverse to a single 4mm diameter straw prototype. We show the arrangement of the single straw prototype and electromagnet in Fig 8.49.

We oriented the straw so that the field was transverse to the straw and irradiated the straw with a Fe55 photon source. The preliminary data on amplitude effects that has been obtained with a 0.75T transverse field on and field off is shown in Fig 8.50 . The gas mixture used was Ar/CO_2 80/20 with the voltage set to 1400V. This was the gas mixture and voltage used for all magnetic field tests. As can be seen (and as was expected), no obvious effect of a transverse field was seen.

Because of the geometry of the single straw prototype and the electromagnet pole tips, it was difficult to obtain the axial field configuration. In order to get a substantial axial field, we have used permanent magnets rather than continue with the electromagnet. A permanent

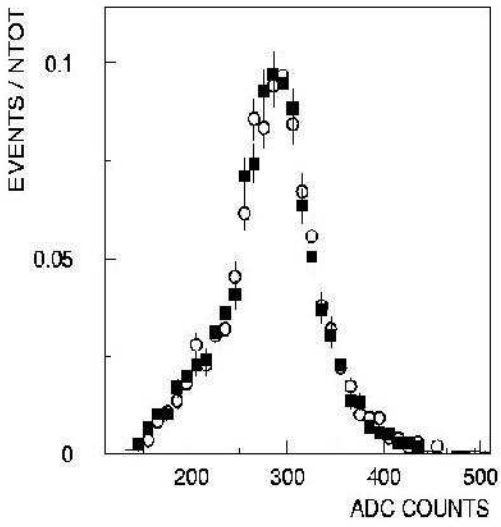

Figure 8.50: Transverse field effect study: Amplitude of signals with transverse magnetic field 0.75T on (circles) and off (squares). Argon-CO_2 80/20 mixture operated at 1400V

magnet array made of segments of Neodymium 35, an alloy of neodymium iron and boron (NdFeB) which has a very high permanent field (residual induction = 1.23T) and good resistance to demagnetization was used. With the arrangement of segments of Neodymium 35 shown in Fig 8.51 , an axial field of 0.52 T was attained as shown in Fig 8.52. This setup will be installed in the test beam.

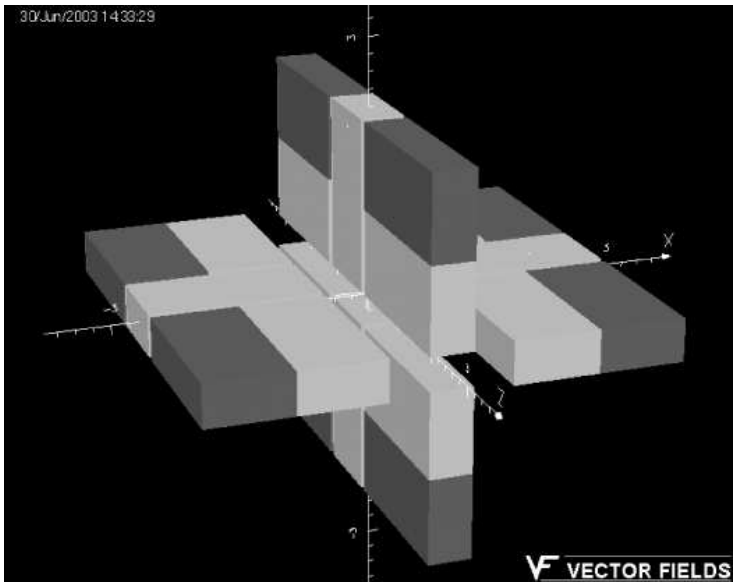

Figure 8.51: Configuration of Neodymium 35 segments to achieve a 0.52T axial field. The light gray segments are the Neodymium 35 pieces and the dark gray are Fe in the arrangement. The axial field is oriented along the z axis.

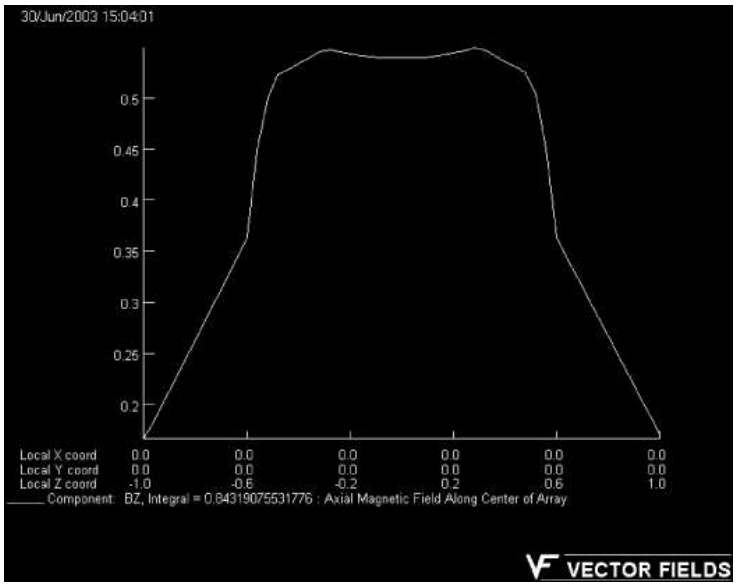

Figure 8.52: Field along the z axis of the Neodymium 35 configuration of Fig. II.4. The units of the vertical axis are Tesla and the horizontal axis are in inches.

8.10 Production, Production Testing, and Quality Assurance Plan

The production of the Straw Detector is broken into major production sites. These sites include the Straw Preparation Site, the Anode Preparation Site, the Module Assembly sites, the Half- View Assembly sites, the Half-View Survey Site, the Electronics Sites, and the Monitor Site. Other work includes miscellaneous systems, fixturing and tooling, and Test Beam Studies. It should be noted that the assigned "Responsible Institutions" are not finalized.

8.10.1 Straw Preparation Site

Responsible Institutions: University of Houston

The Straw Preparation site is responsible for receiving the straws, and wire centering devices from the manufacturers, quality control, and producing a straw of the correct length for a given station. The quality control on a straw will include a test for leak tightness, cathode continuity, and straightness, before any preparation work is done. Some small fraction of the straws will be placed under environmental tests to insure that our mechanical model of the straw remains true. The quality control on a wire centering device will be done through sampling methods. The parameters of interest are the depth of the centering groove, and a surface quality check. A "finished" straw will have the wire centering devices inserted to the prescribed depth for a given module and station number. The Straw Production versus Station number will be monitored via a database so that the Straw production will keep the supply of straws to the Module Assembly Site sufficient so that an orderly schedule of Half-Views Assemblies can continue.

8.10.2 Anode Preparation Site

Responsible Institution: University of Virginia, Southern Methodist University

The Anode Preparation Sites are responsible for receiving the anode wire and glass capillary tubes from the manufacturers, quality control, and production of completed anode wires of the correct length for a given station. The quality control will include testing the anode wire for diameter, smoothness, tensile strength, and conductivity. These tests will be done using sampling methods. A "finished" anode will be composed of insulated segments of wire fused together by a glass capillary. Depending upon the particular module number in a station, there may be either two or three wire segments per anode. The Anode Production versus Station and module number will be monitored via a database so that the anode production will keep an orderly supply of anodes flowing to the Half-View Sites.

8.10.3 Module Assembly Sites, including MOX-Silicon Support

Responsible Institutions: University of Virginia, Fermilab, Frascati

The module assembly site receives the straws from the Straw Preparation site, the straw end-plugs and module endplates from the manufacturers. Quality control is done on the end-plugs (by sampling) and on the module endplates by explicit measurements. A "finished" module will be composed of 48 straws, with glued end-plugs, and glued to two module endplates. The gluing will be done with silver epoxy which provides the electrical connection from the module end-plate to the straw cathode. Quality control on a module will include a leak test and cathode continuity to the end-plate. Since the straw material is sensitive to environmental conditions, it is important that a strict control be made on the relative humidity and temperature of the assembly room at the time the module is glued. This information will be recorded into the production database along with the module ID.

The special X modules(MOX) for supporting the silicon strip stations will be constructed at Frascati.

8.10.4 Half-View Assembly Sites

Responsible Institutions: University of Virginia, Fermilab

The Half-View Assembly Site receives the modules from the Module Assembly Sites, the anodes from the Anode Preparation Site, the Half- View Frames, the High Voltage Network (HVN) card from the manufacturer, the anode pinning block from the manufacturer, and other various and sundry items necessary for the Half-View Production. If not already done, the HVN card will be burned in for high voltage, otherwise high voltage testing will be done on a sampled set of cards. The Half-View Frames will be quality controlled by direct measurements of the frames. A Half-View will be constructed by inserting the appropriate modules, along with the anode pinning block into the Half-View frame. At this point, the frame can be tensioned, leak tested, and repaired if needed. Then the anodes will be strung. The tension in the anode will be measured online and stored in a database. If the tension is outside limits, the anode can be redone. When a module (or a group of modules) in a Half-View has been strung, it can then be tested for proper operation by flowing a non-flammable chamber gas. In order to do this, the HVN card and a Front End Electronics Board (containing a preamp and a discriminator) must be attached to the frame at the module site. By using a radioactive source, we can count pulses to check that the operation is within specifications. This will be recorded into a database. If the module is outside specifications, repair can then be done. A "finished" Half-View will then be put into storage, with a supply of dry nitrogen gas attached to the input gas supply.

8.10.5 Electronics Sites

Responsible Institution: Fermilab, University of Virginia, Southern Methodist University, University of Houston

The Electronics Sites are responsible for production and testing of the Front End Electronics Boards: the High Voltage Network (HVN) card, the High/Low Voltage Bus (H/LVB), the Preamp-Discriminator Board (PDB), the Time to Digital Converter (TDC) board. The

HVN card receives positive high voltage from HV power supplies, and buffers it through a load resistor to all straws in a given module. The HVN card also provides high voltage blocking capacitors to the PDB such that the preamp inputs can operate at a virtual ground. The HVN cards will need to be "burned in" in order to insure that they can hold off the high voltage. The H/LVB distributes the high and low voltages inside the frame. The PDB will contain the preamplifier/ discriminator. The TDC board contains not only the TDC function, but also miscellaneous control and communication circuitry to the Data Combiner Boards (DCB). These functions may be implemented in custom circuitry. Quality control on each element will be made before installation in the Half-View Detector. The entire front end system will undergo complete testing at the Survey Site.

8.10.6 Survey Site

Responsible Institution: Fermilab

The Survey Site receives the finished Half-Views from the Half-View Assembly Site. Its function is to measure the location of the anode wires at a point close to the wire centering devices inside the straws with respect to a know set of fiducials on the Half- View Frame. If this wire location is known at each wire centering device site, then the wire position along the straw is simply a straight line between adjacent wire centering devices. This data will be recorded and stored in a database, which will eventually be part of the Straw Detector geometry. The entire front end electronics system will also undergo complete testing at the Survey Site.

8.10.7 Gas and Environmental Monitoring Site

Responsible Institution: Southern Methodist University

The Straw Detector measures position in the straw by determining the time between the interaction and the time the drifting electrons arrive at the anode wire. This drift time can be sensitive to the molecular density of the gas inside the straw. This density depends upon the temperature and atmospheric pressure. The monitoring of the drift speed will take place in several monitors. One monitor will measure the barometric pressure and temperature in the C0 Pit. Another monitor will actually measure the drift speeds in the chamber gas.. Another concern with the Straw Detector is the aging which may occur in the high occupancy straws near the beampipe. We will have gas monitor detectors in which the aging is accelerated by external radioactive sources. We will measure the gain (which is sensitive to aging effects) in these detectors both before the gas enters and after the chamber gas exits the Straw Detector. Any aging seen in these detectors will pre-alert us to problems before they actually occur in the Straw Detector. The straw material is very sensitive to both temperature and humidity. Since the straws are held in place by externally tensioning the straws on the Half-View Frame, it is necessary to keep the Straw Detector within temperature and humidity limits. It will be necessary to monitor these quantities both globally in C0 as well as internally in each sealed Half- View. In case the humidity or temperature climbs outside of tolerances,

the Straw High Voltage must be turned off in order to prevent damage. This Environmental monitor will be responsible for these actions.

8.10.8 Other Systems

Responsible Institution-Fermilab, Frascati, University of Houston, University of Virginia, Southern Methodist University

These systems include the gas system for the straws, the cooling system for the frames and electronics, high and low voltage power supplies and supporting cabling. The quality control on these systems will be done as they are designed and built, or when they are received.

8.10.9 Various tooling and fixtures

Responsible Institutions- Fermilab, Frascati, University of Houston, University of Virginia, Southern Methodist University

All the previous sites will depend upon an infrastructure of tooling and fixtures, including the mechanical design and assembly of the half-view frames. This equipment will be prototyped and designed prior to the start of production. To a great extent, we will rely on previous designs from the Atlas Straw Collaboration, adapted to our particular needs. At this time it appears that the tooling will be constructed at the site where it is expected to be used.

8.10.10 Test Beam Studies

Responsible Institutions- Fermilab, Frascati, University of Houston, University of Virginia, Southern Methodist University

Various beam tests will be done using both prototypes and actual production Half-Views. All the Straw Collaboration members will participate in the Test Beam setups, runs, and analysis.

Bibliography

[1] ATLAS Inner Detector Technical Design Report, CERN/LHCC/97-16,17.

[2] D. Olis, "Load Test of Short Prototype Struts for the BTEV Straw Frame ", BTeV Doc 2475

[3] M. Caponero et al., "Use of Fiber Bragg Grating Sensors for detector position monitoring", BTeV Doc 1297.

[4] M. Caponero et al., "Composite Materials for FBG", BTeV Doc 1064

[5] T. Tope, "BTeV Straw Gas System ", BTeV Doc 259

[6] F.M. Newcomer, R. Van Berg, J. Van der Spiegel and H.H. Williams, Nucl. Instrum. Meth. A 283 (1989) 806.

[7] Results of tension tests for various gases are described in BTeV internal documents:
P. Kasper, "Straw Tension for different gas mixtures", BTeV Doc 1686,
B. Nitti, "Axial Stretch, Temperature, and Humidity Effects on Straw Sag", BTeV Doc 2610,
F. di Falco, "Study of tensile response of kapton and mylar strips to Ar and CO2 mixtures", BTeV Doc 2361

[8] R. Veenhof, "Garfield Version 7.02" CERN-CNL-2000-001, Vol XXXV, issue no 1, http://garfield.web.cern.ch/garfield

[9] "Aging in large cdf tracking chambers ", M. Binkley *et al.*, FERMILAB-CONF-02-041-E, Mar 2002, and references therein. To be published in Proceedings of International Workshop on Aging Phenomena in Gaseous Detectors, Hamburg, Germany, 2-5 Oct 2001.

[10] "Aging studies of cms muon chamber prototypes ", T. Ferguson et al., Nucl.Instrum.Meth. **A 488**,240-257,2002;

[11] "Aging studies for the Atlas transition radiation tracker (TRT)", T. Akesson *et al.*, Oct 2001, to be published in Proceedings of International Workshop on Aging Phenomena in Gaseous Detectors, Hamburg, Germany, 2-5 Oct 2001;

[12] "Aging properties of straw proportional tubes with A XE-CO-2-CF-4 gas mixture ", M. Capeans *et al.*, Nucl.Instrum.Meth.**A337**, 122-126,1993;